2013

Health Diagnosis of Lithium-ion Battery Cell Using Vibration-based Test and Analysis

Huan Le Pham
Purdue University

Graduate School ETD Form 9
(Revised 12/07)

PURDUE UNIVERSITY
GRADUATE SCHOOL
Thesis/Dissertation Acceptance

This is to certify that the thesis/dissertation prepared

By Huan Le Pham

Entitled
Health Diagnosis of Lithium-ion Battery Cell by Using Vibration-based Test and Analysis

For the degree of Master of Science in Mechanical Engineering

Is approved by the final examining committee:

Dr. Douglas E. Adams	Co-Chair		
Chair			
Dr. Farshid Sadeghi	Co-Chair		
Dr. James Eric Dietz			

To the best of my knowledge and as understood by the student in the *Research Integrity and Copyright Disclaimer (Graduate School Form 20)*, this thesis/dissertation adheres to the provisions of Purdue University's "Policy on Integrity in Research" and the use of copyrighted material.

Approved by Major Professor(s): Dr. Douglas E. Adams

Dr. Farshid Sadeghi

Approved by: Dr. David C. Anderson 12/04/2013

Head of the Graduate Program Date

HEALTH DIAGNOSIS OF LITHIUM-ION BATTERY CELL USING VIBRATION-BASED TEST AND ANALYSIS

A Thesis

Submitted to the Faculty

of

Purdue University

by

Huan Le Pham

In Partial Fulfillment of the

Requirements for the Degree

of

Master of Science in Mechanical Engineering

December 2013

Purdue University

West Lafayette, Indiana

To Mom and Dad

ACKNOWLEDGMENTS

First, I would like to thank my adviser Dr. Douglas E. Adams for his guidance, tremendous enthusiasm, and patience throughout my endeavor. I also would like to thank my thesis committee, Dr. Farshid Sadeghi for his commitment and support; and thanks to Dr. J. Eric Dietz for his valued information and equipment that made this work possible. Thanks to all of my colleagues at PCSI Kepner. It was a great honor to be a part of such an amazing and talented group of individuals, and I'm so proud to be one of the Kepnerians. Finally, I would like to thank my sponsoring organization, Sandia National Laboratories, for providing funding for my study. Sandia National Laboratories is a multi-program laboratory managed and operated by Sandia Corporation, a wholly owned subsidiary of Lockheed Martin Corporation, for the U.S. Department of Energy's National Nuclear Security Administration under contract DE-AC0494AL85000.

TABLE OF CONTENTS

LIST OF TABLES

LIST OF FIGURES

SYMBOLS

ϵ_r	Radial strain in electrode particle
ϵ_t	Tangential strain in electrode particle
θ	Angular Displacement (Rad)
$\ddot{\theta}$	Acceleration (Rad/s^2)
ν	Poisson's Ratio
ρ	Density (kg/m^3)
σ	Stress (MPa)
σ_r	Radial Stress in Electrode Particle (MPa)
σ_t	Tangential Stress in Electrode Particle (MPa)
Ω	Theoretical partial molar volume of Li-ion (cm^3 mol^{-1})
ω	fractional expansivity of electrode material
A_e	Element Cross-section Area (m^2)
$[C]$	Damping Matrix
C_{rate}	Rate of Charge/Discharge
c_s	Ion Concentration in Solid Phase (mol L^{-1})
E	Elastic Modulus (MPa)
f_e	Elemental Force (N)
F	Faraday's constant (96487 C mol^{-1})
$[F]$	Force Input Matrix
h_o	Initial electrode thickness (m)
h_{max}	maximum electrode thickness (m)
$H(j\omega)$	Frequency Response Function
I	Electric Current (A)
I_e	Elemental Moment of Inertia (Kg.m^2)
$[K]$	Spring Stiffness Matrix

L	Beam Length (m)
I_e	Beam Element Length (m)
M_e	Elemental Moment (N.m)
$[M]$	Mass Matrix
N	Number of electrode layers in a single cell
Q	Capacity (Ah)
t	Time (s)
u	Translational Displacement (m)
$\dot{u}$	Translational Velocity (m/s)
$\ddot{u}$	Translational Acceleration (m/s^2)
x	Stoichiometric Number in anode
y	Stoichiometric Number in Cathode

ABBREVIATIONS

DAQ	Data Acquisition
DMA	Dynamics Mechanical Analyzer
FBD	Free Body Diagram
FEM	Finite Element Method
FFT	Fast Fourier Transform
FIR	Finite Impulse Response
FRF	Frequency Response Function
IFFT	Inverse Fast Fourier Transform
IIR	Infinite Impulse Response
LIB	Lithium-ion Battery
MIMO	Multiple Input Multiple Output
NDT	Non-Destructive Testing
PMS	Power Management System
SHM	Structural Health Monitoring
SIMO	Single Input Multiple Output
SOC	State of Charge
SOH	State of Health

ABSTRACT

Pham, Huan Le M.S.M.E., Purdue University, December 2013. Health Diagnosis of Lithium-ion Battery Cell Using Vibration-based Test and Analysis. Major Professor: Dr. Douglas E. Adams, School of Mechanical Engineering.

With their superior advantages of high capacity and low percentage of self-discharge, lithium-ion batteries, which are most commonly used as power sources for hand-held electronic devices, have become the most popular choice for power storage in electric vehicles. Due to the increased potential for long life of lithium-ion batteries in vehicle applications, manufacturers are pursuing methodologies to increase the reliability of their batteries. Methods are now being developed to monitor the health of lithium-ion batteries throughout their life cycle. The work in this thesis is focused on utilizing non-destructive vibration diagnostic testing methods to monitor changes in the physical properties of the lithium-ion battery electrodes, which dictate the states of charge (SOCs) and states of health (SOHs) of the battery cell. Inside a lithium-ion battery cell, lithium ions travel from cathodes to anodes during charge and reverse during discharge; these processes transfer matter from one electrode to another causing mechanical properties such as thickness, mass, and stiffness of the electrodes inside a battery cell to change at different states of charge; therefore, the detection of these changes will serve to determine the state of charge of the battery cell. As mass and stiffness of the electrodes change during charge and discharge, they will respond to the excitation input differently. An automated vibration diagnostic test is developed to characterize the state of charge of a lithium-ion battery cell by measuring the amplitude and phase of the kinematic response as a function of excitation frequency at different states of charge of the battery cell and at different times in the life of the cell. Also, the mechanical properties of the electrodes are obtained by direct measurements to estimate the thickness change at different SOCs and to

develop a first-principles frequency response model for the battery cell. The correlation between the vibration test results and the model will be used to determine the exact SOC of the battery cell.

1. INTRODUCTION

1.1 Motivation

Lithium-ion batteries (LIBs) have been increasingly used for power storage in a wide range of applications since they were first commercialized by Sony in 1991. LIBs were accepted immediately after they were introduced to the market because they possess performance attributes that other battery types lack [1]. LIBs have quickly assumed a dominant position in the market. In 2009, the sales of LIBs were estimated to be over 4 billion units; and sales are expected to be doubled by 2015 [2]. With their high energy density, LIBs can hold much more energy and possess less overall weight compared to other battery types; therefore, LIBs have met the demand for high capacity and lightweight batteries for use in compact electronic devices. Moreover, with excellent life cycle and no memory effect, LIBs have become the best choice in energy storage used in transportation applications. LIBs used in electric vehicles and commercial aircrafts can be constantly cycled without having the risk of losing capacity due to not being fully charged or discharged. Although there is tremendous potential for LIB technologies to gain even more market share in the future, there are some disadvantages that concern battery manufacturers and users, regarding reliability and cost. To addressed these concerns, the processes for developing and manufacturing LIBs are being rapidly improved to increase the battery capability and efficiency. However, the technologies for inspecting and monitoring the quality and health of LIBs have not been developed at the same pace. The health of a LIB can be characterized by its states of charge (SOCs) and total capacity throughout its life cycle. Currently, there are several methods that are used to estimate the SOCs of LIBs including measuring terminal voltage, impedance during discharge, or by Coulomb counting [3; 4]; however, as discussed in [4], there are drawbacks with

those methods as errors often occur in measurements when the relationship between SOC and terminal voltage is assumed to be a linear relationship, and the losses in current measurements are not taken into account. Also, current technologies do not have a reliable method to determine the states of health (SOH) of LIBs which is crucial in power management system (PMS) in transportation applications. There are many factors that affect the performance and health of LIBs in service such as manufacturing defects, environmental factors, users' habits, etc. Moreover, the cost to produce LIBs is high due to the complicated manufacturing and quality control processes of the battery cells. The processes require high precision in manufacturing and assembling the electrodes inside a battery cell because small variations of electrodes will affect the overall performance and health of a battery cell [5]. A recent study sound that the total costs of producing LIBs for electric vehicles are estimated at $17,000 per unit [6]. This high cost of the battery units will drive up the overall costs of an electric vehicle. Therefore, it is essential to develop a low cost and effective testing method to monitor the SOC and SOH of the batteries through changes in physical properties of electrodes to reduce the manufacturing cost, improve the battery performance, and detect any problem that might occur during service in the future.

1.2 Review of Past Work

There are several factors can cause degradation in the performance and health of a LIB cell ranging from manufacturing defects to working environments, and users' habits. The major components inside the battery cell are directly affected by those factors. Defects and damage change the compositions of the materials and physical conditions of those components which will ultimately result in the degradation of the performance and health of the battery cell. As the LIB industries and consumers become more aware of the fact that chemical and physical properties of the LIB cell components such as electrodes and electrolytes are the keys to detect damage and to

monitor the health of a LIB cell, there are new technologies being developed to provide the LIBs industries the useful tools which can be used for testing and monitoring the LIBs to improve the quality and lower the cost of the batteries. Nondestructive testing (NDT) methods have been used in many structural health monitoring (SHM) systems to detect changes or damage of a structure. Those methods have the potential to become the perfect solution in LIB health monitoring because they are designed to obtain accurate measurements of the samples without destroying or introducing additional changes to the original structures.

Sharp (2012) [7] developed a technique to detect faults and defects in composite electrodes of LIBs using flash thermography technology. In order to examine the quality of an electrode, an electrode sample is placed between a high energy flash bulb and an infrared thermal camera. As the heat pulse from the flash energy penetrates the electrodes materials, the infrared camera will pick up the thermal signature from the electrode's surface. Thus, any defect and damage can be revealed by analyzing the differences in amplitudes of the thermal response measured from the electrode. This technology is very effective in detecting the electrode's defects by analyzing the non-uniformity in thermal signatures of an electrode. However, it is limited to the electrodes' manufacturing stage because the measurement can only be performed on the opened electrodes and not the ones which have already been assembled inside a LIB cell. Therefore, it lacks the capability of real-time examining the electrodes' properties changes as well as monitoring the health of a LIB cell throughout its life cycle. In a study by Smith et al (2009) [8], a numerical model is developed to simulate the effects of randomness of shape, morphology, and packaging of LIB electrode's cross-section on the electrochemical behavior which affects the overall charge capacity of a LIB cell. The results from the model show that electrodes' particle-size distribution, clustering, surface roughness affect Li-ions concentrations on the anode surfaces and induce polarized losses which decrease capacity of the LIB cell. The findings from this study provide useful information about how manufacturing processes of electrodes' materials and the battery cell's assembly can affect the total charge capacity of a LIB

cell; however, this study does not provide a practical method to examine the quality of a battery cell before and during service so that the SOH of a LIB can be evaluated.

Also, there are several efforts to examine the physical conditions of components inside a LIB cell during service because the changes in physical conditions of battery cell's components are directly related to its SOCs and SOHs. It is very difficult to obtain the exact measurements of the internal components of a battery cell because they are inaccessible inside an active LIB cell, and most of their properties changes are often too small to be able to detect using conventional measuring techniques. The most explorable parameter of a battery cell is the change in its volume during charge and discharge processes. In a study by Wang et al (2004) [9], in-situ methods using both load cells measurement and X-ray observation are used to investigate the volume change in LIB cells during charge and discharge. To measure the volume change of a whole battery cell, the cell is clamped between 2 spacers, strain gages are attached between the interfaces of the spacers and both sides of the battery cell. As the battery cell is cycled, any change in its volume will reflect by the change of the strain gages. Also, an X-ray inspection system was used to examine the volume change of electrodes during cycle. The study found that the volume change of a LIB cell correlates with the number of cycles as the volume change is increased with cycling in the life cycle test; thus, there are irreversible changes in electrodes properties as the number of cycles increases leading to the degradation of the battery cell. The results from this study clearly show the relationship between volume change and life cycle of a LIB cell, and it might help to determine the SOHs of a LIB cell based on the amount of permanently increased volume. However, the experiments set up are complicated and costly make it difficult to efficiently utilize in practical applications. In another work by Fu et al (2012) [10], a model of mechanical stress in the electrodes is developed based on electrodes' thickness changes during charge and discharge. This model can be used to monitor mechanical stresses on the electrodes inside a LIB cell as the total thickness of the cell is measured using two linear voltage displacement transducers (LVDT) during charge and discharge. Results from this study found "the magnitude

of stress depends upon locations and C_{rate}, while the thickness of a single cell is mainly affected by the state of charge (SOC),but not C_{rate}". The work in this study provides very useful information to estimate thickness change and stress on the electrodes as the battery cell is cycled. However, using LVDT on a soft and uneven surface of a LIB cell may not be adequate to describe the thickness change of the whole battery cell because LVDT is a single point measurement; thus, the stress estimated using LVDT only represents the stress at that point and not the whole battery cell.

1.3 Approach

Vibration-based testing techniques are one type of NDT methods which have been used in many SHM systems to detect changes or damage to a structure by first diagnosing the damage of the system, and developing a prognosis for the system to predict the conditions or problems of the system in the future [11]. In SHM systems, damage of a structure can be identified by measuring and analyzing its changes in the kinematic response [12]. If a structure or object can be visualized as a system of masses, springs, and dampers, then the system will vibrate due to a forced excitation; therefore, the magnitude and phase of the frequency response function (FRF) can be measured from the kinematic response of the system. By using this technique, a LIB cell can be treated as a mechanical system with its mass, spring, and damper. Thus, when the battery cell is charged or discharged, there is a change in the system, it is assumed that the change will result in changes of the FRF of the system. Therefore, the FRF reflects the condition of the system as the FRFs of the LIB cell are related to the physical properties of the electrodes and other components inside the cell. The changes of the FRF magnitude and phase of the system will help to determine the SOC and SOH of the LIB cell.

Also, the actual physical properties of electrodes are obtained by direct measurements of each electrode at different SOCs to learn about the relationship between the cell SOC and its electrodes' physical properties changes. The measured electrodes'

properties are used for developing a physics-based frequency response model of the cell. The model and the results from vibration tests will be used to form the FRF pattern of the battery cell with different conditions based on the changes in electrodes' properties, and the results will be used to determine and predict the performance and problems of LIB cells in the future.

1.4 Thesis Statement

This thesis will develop a new vibration based method utilizing vibration diagnostics testing and finite element modeling to use as a low cost and effective way to monitor the SOCs and SOHs of a LIB cell.

The hypothesis is that the electrodes' thickness will change during a battery cell's cycle. The thickness will be decreased in the cathode and increased in the anode during charge and reserved during discharge. The changes in the electrodes' thickness will result in the change in the whole structure of a LIB cell. Therefore, the battery cell will respond to an excitation input differently at different change. By characterizing the changes of a LIB cell during its cycle using vibration test, the SOCs and SOHs of a LIB cell will be obtained.

The advantage of this method is it can characterize the SOCs and SOHs of a LIB cell with very small variation of its components properties by analyzing the structural changes of the materials. Different defects or damage will introduce distinct changes in the structure of a system causing it to vibrate differently when an excitation is applied. Therefore, capturing the FRFs of a LIB cell from vibration tests will provide information which will be used to adjust the parameters in the dynamics model to produce FRFs which correlate to the ones from test results; thus, the source of change can be identified. By implementing vary parameters, this method can be used as a prognosis tool to predict the health of a LIB cell during service.

2. LITHIUM-ION BATTERY CELL STRUCTURE AND OPERATION

A LIB cell is a complicated system; the structure of a single cell contains several different components with different material compositions. Inside a LIB cell, chemical compositions and physical properties of its components are constantly changed with different rates due to chemical reactions between active materials; the rate of change of components' properties is very low as the battery cell is in idle state and high during cycle; the rate of change increases when the rate of charge/discharge (C_{rate}) increases. For a rechargeable LIB cell, the changes in its components' properties during cycle have to be reversible; in other words, the materials properties of electrodes, which are changed after the cell is charged, are able to restore to their previous conditions after it is discharged and vice versa. Permanent changes to the cell's components properties will result in irreversible capacity loss and even failure of the cell.

Figure 2.1: A LIB Cell.

A fully assembled and functional LIB cell is shown in Figure 2.1. This is the high capacity prismatic LIB cell commonly used as power sources in transportation applications, especially electric vehicles. There are multiple LIB packs are used to

provide power for an electric vehicle, and each pack consists of 24 to 48 battery cells to provide enough voltage to power the vehicle. A battery power system in an electric vehicle is a very sensitive system because everything in the system has to work consistently all together; if one component is damaged or fails, it will lead to the failure of the whole system. As a LIB pack is cycled, every cell in the pack receives the same charge/discharge conditions. Therefore, if one cell loses its capacity or gets damaged, it will be destroyed from being excessively charged/discharged, and the whole system will be severely damaged. Thus, to be able to detect LIB cell SOCs and SOHs will help to determine the health conditions of the battery cell's internal components and will help to prevent catastrophic failure of the whole system. It is important to understand the construction and operation of a LIB cell in order to investigate the effects of its components' material properties to its performance and health.

2.1 Structure and Components of a Lithium-ion Battery Cell.

There are three functional components inside a LIBs cell: they are the cathode, anode, and electrolyte. Figure 2.2 shows the internal structure of a LIB cell and the order of its electrode layers. Inside a LIB cell, layers of cathodes and anodes are alternatively stacked on top of each other to increase the surface area to maximize the capacity of the cell. Micro-porous polymer separators are inserted between the electrodes to allow Lithium-ions to move between them. The battery cell operates through the interactions between the electrodes as electrochemical reactions occur between active materials and the electrolyte on the electrodes' surfaces. Therefore, the charge and life cycle of the battery cell are dependent on the conditions of the interfaces between the electrodes [13].

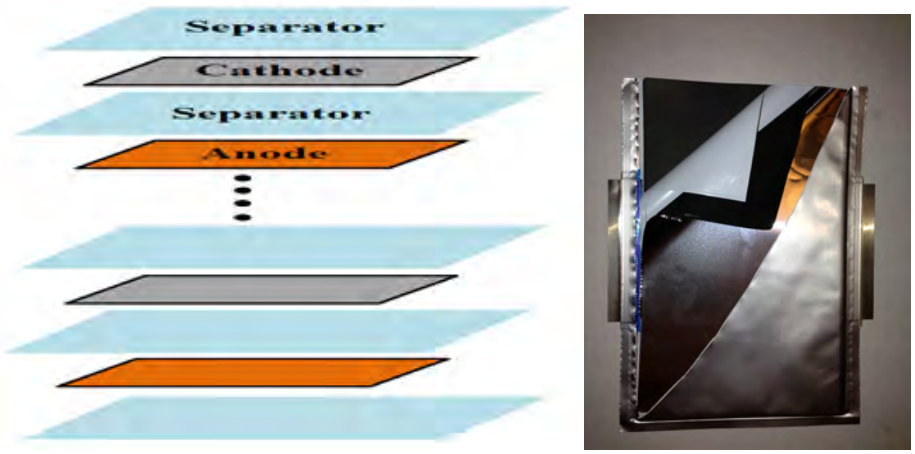

(a) (b)

Figure 2.2: (a) Electrodes Stacking Order in a LIB Cell; (b)Components Inside a LIB Cell.

2.1.1 Cathode

The cathode is the positive electrode inside the battery cell which contains positive materials, typically a metal oxide with layered structure, or a material with tunneled structure and are coated on an aluminum film current collector. In most commercial LIB cell, positive electrode materials are coated on both sides of the aluminum current collector to increase the surface area which will improve the efficiency of the LIB cell when the electrodes are stacked inside the battery cell.

Because the majority of Li-ions are concentrated in the positive electrode materials, cathodes play a critical part in the overall performance and health of a LIB cell. Because their materials properties go through intensive structural changes during cycle, positive electrode materials must satisfy a set of requirements which are summarized in Table 2.1 [2]. Figure 2.3 shows the structure of a cathode after coated with active electrode materials.

For years, LIB researchers and manufacturers have faced tough challenges to come up with positive electrode materials that satisfy most of the requirements in Table 2.1 and yet still be safe for applications because they are often contradicting one another.

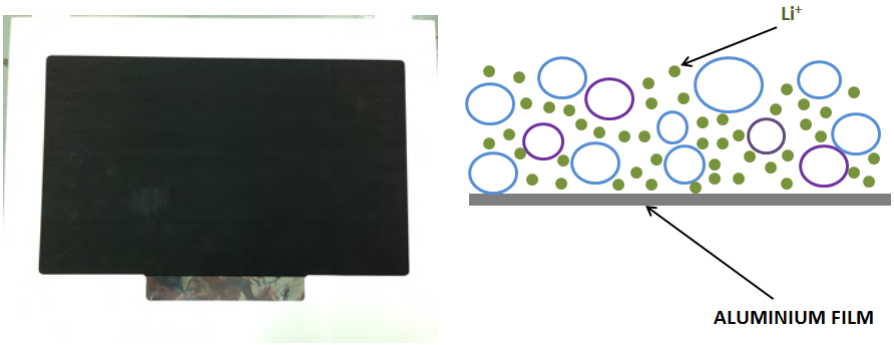

(a) (b)

Figure 2.3: (a) Double-side Coated Cathode. (b)Positive Electrode Materials Coating Layer of Cathode.

Table 2.1: Positive Electrode Materials Requirements. [2]

High free energy of reaction with lithium
Can incorporate large quantities of lithium
Reversibly incorporates lithium without structural change
High lithium ion diffusivity
Good electronic conductivity
Insoluble in the elctrolyte
Prepared from inexpensive materials
Low-cost synthesis

There are many ways to increase the capacity of a LIB cell. One of the most efficient ways is to increase the specific energy of the positive electrode materials. In order to increase their specific energy, larger amount of Li-ions are inserted into the positive electrode materials. As a result, the systhesis cost will increase because it is difficult to insert more Li-ions into a high density structure. Moreover, Lithium is a highly reactive metal. Lithium will react intensively with water or moister to form metal hydroxide solution. The reaction will generate heat and Hydrogen gas. Therefore, higher capacity positive electrode materials might have higer risk of rupture and fire than that with lower capacity in case of active materials are exposed to the open

air due to defect or damage occurs. Thus, there are different types of the positive electrode materials for different purposes. The characteristics of common positive electrode materials are described in Table 2.2 [2]; the positive electrode materials are selected based on the applications and working environments of the battery cells.

Table 2.2: Characteristics of Common Positive Electrode Materials. [2]

Material Composition	Specific Capacity mAh/g	Midpoint V v.s. Li at C/20	Comments
$LiCoO_2$	155	3.9	Still the most common, but Co is expensive.
$LiNi_{1-x-y}Mn_xCo_yO_2(NMC)$	140-180	~3.8	Safer and less expensive than $LiCoO_2$,Capacity depends on upper voltage cutoff.
$LiNi_{0.8}Co_{0.15}Al_{0.05}O_2$	200	3.73	About as safe as $LiCoO_2$, high capacity
$LiMn_2O_4$	100-120	4.05	Inexpensive, safer than $LiCoO_2$, but poor temperature stability.
$LiFePO_4$	160	3.45	Synthesis in inert gas leads to process cost. Very safe, low volumetric energy.
$Li[Li_{\frac{1}{9}}Ni_{\frac{1}{3}}Mn_{\frac{5}{9}}]O_2$	275	3.8	High specific capacity.
$LiNi_{0.5}Mn_{1.5}O_4$	130	4.6	Requires an electrolyte that is stable at a high voltage

2.1.2 Anode

The anode is the negative electrode inside a battery cell. The typical material used in the anode is a graphitic carbon which is coated on a thin copper foil current collector, Figure 2.4. Similar to the cathode, the anode materials are coated on both sides of copper current collector to increase the efficiency when the electrodes are stacked inside the battery cell. The anode materials are designed so that they can receive the maximum amount of the Li-ions removed from cathodes during charging; therefore, any defect or damage on the anode surfaces will affect the performance and health of a battery cell as Li-ions are unevenly or overly distributed.

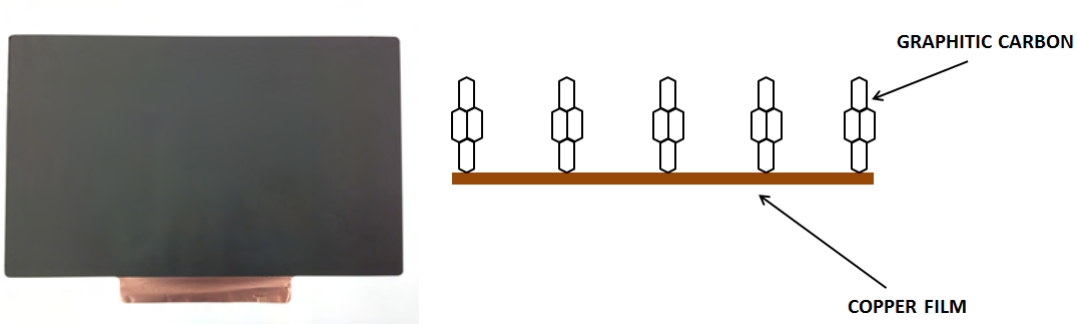

(a) (b)

Figure 2.4: (a) Double-size Coated Anode. (b) Negative Electrode Structure.

2.1.3 Electrolyte

The electrolyte is the chemical compound which bridges the electrodes providing pathways for Li-ions to travel as the cell is cycled. There are two main types of electrolytes in common LIB cell: liquid and gel electrolytes. Liquid electrolytes are solutions of a lithium salt in organic solvents such as carbonates, and they are most commonly used in commercialized LIBs because they are very practical and efficient in LIBs manufacturing as battery electrodes are wetted with the exact amount of electrolyte before they are packaged inside the cell.

Table 2.3 [2] lists common Lithium salts currently used in Li-ion electrolytes in most of commercial LIBs today. Electrolyte plays an important role in a LIB cell because it serves as connection to link electrodes together. Therefore, degradation in electrolyte will result in capacity loss and even failure of the battery cell. The most common defects and degradation caused by electrolyte in a LIB cell occur when there are present of impurities such as water or HF inside a battery cell. These impurities will cause electrolyte oxidation at the positive electrodes and degrade the electrode materials. This oxidation will result in irreversible capacity loss. Also, those oxidation reactions can produce gases that will increase the pressure inside the pouch and lead to severe damage, especially for the prismatic battery cells.

Table 2.3: Common Salts Used in Li-ion Electrolytes of LIB Cells. [2]

Name	Formula	Mol.Weight (g/mol)	Typical Impurities	Comments
Lithium hexafluorophosphate	$LiPF_6$	151.9	H_2O, HF	Most Common
Lithium tetrafluoroborate	$LiBF_4$	93.74	H_2O, HF	Less hygroscopic than $LiPF_6$
Lithium bisoxalatoborate	$LiB(C_2O_4)_2$	193.7	H_2O	Good for solid electrolyte interface (SEI)
Lithium bistrifluoromethane sulfonimide	$LiN(CF_3SO_2)_2$	286.9	H_2O	Help reduce gassing and improve high temperature life cycle

2.2 Operation of a Lithium-ion Battery Cell

2.2.1 Intercalation Processes

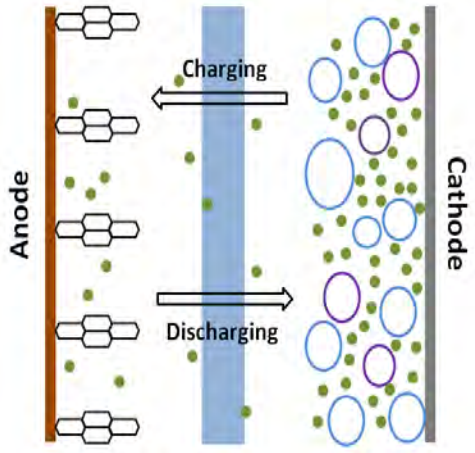

Figure 2.5: Intercalation Process between Cathode and Anode.

A LIB cell operates based on the intercalation processes which is demonstrated in Figure 2.5. As a LIB cell is charged, current flows from positive to negative electrodes which causes Li-ions to travel from cathodes to anodes and reverse when the battery cell is discharged. Therefore, the electrodes' structures are designed to sustain the intercalation process so that when Li-ions are removed from and inserted to the host materials, they will not cause any significant change in the host structure. If there is any irreversible change in the host materials, there will be loss in charge capacity and failure of the battery cell.

2.2.2 Lithium-ion Battery States of Charge

The state of charge (SOC) of a LIB battery is defined as the percentage of the total capacity a battery cell can hold [14]; As the LIB cell is cycled, Li-ions travel from one electrode to another; the amount of ions transported between the electrodes determines the charge of a LIB cell. At the end of each cycle, there is a maximum amount of Li-ions that can be transported from one electrode to another; this is referred to as the total capacity of a LIB cell (Q). Therefore, the SOC is an indication of the amount of Li-ions presents in both cathodes and anodes; and the changes between the SOCs represent the amount of Li-ions transported from one electrode to another. Also, the physical properties of electrodes' materials can be determined from the amount of Li-ions transported between electrodes; as a result, to be able to measure the exact SOCs of a LIB cell will also measuring the physical properties changes of the electrodes inside the cell.

The exact SOC of a battery cell can be calculated as [14];

For charging:

$$SOC_{k+1} = SOC_k + \frac{\int_{t_k}^{t_{k+1}} I(t)dt}{Q} \times 100. \tag{2.1}$$

For discharging:

$$SOC_{k+1} = SOC_k - \frac{\int_{t_k}^{t_{k+1}} I(t)dt}{Q} \times 100. \tag{2.2}$$

$I(t)$ from equations (2.1) & (2.2) is the electric current as a function of time, and k is an integer as the percentage of the SOC ($k = 0, 1, ..., 99$). So, when the electric current is a constant value, equations (2.1) & (2.2) can be simplified as:

$$SOC_{k+1} = SOC_k \pm \frac{I \times t}{Q} \times 100. \tag{2.3}$$

Thus, the exact SOCs of a LIB cell can only be measured when the battery cell is charged or discharged with constant current. However, in practical applications using batteries, the current is always changed with time; therefore, it is very difficult to measure the exact SOCs of the battery because it requires a measure of the exact current values at different times.

The information in this chapter will provide a basic understanding about the fundamental of LIB, and this information will be used to develop a technique to investigate the SOCs and SOHs of the LIB.

3. EXPERIMENTAL METHODS

At each SOC, there is some amount of Li-ions that are transported from one electrode to another. As a result, there are changes in physical properties of the electrodes such as mass, stiffness, thickness, and density. If a LIB cell is considered as a mass-spring-damper system, the changes in the system will reflect through changes in the FRF of the system. The vibration test is designed to obtain the FRF of the LIB cell at different SOCs. By applying an excitation force to the LIB cell at each SOC, the accelerometer will pick up the acceleration response from the battery cell as it vibrates. The information obtained from the force input and the acceleration output is used to estimate the FRF of the battery cell at that SOC. Thus, the FRF obtained from the vibration test can be used as an indicator to determine the changes in the structure of the LIB cell.

3.1 Apparatus

Testing equipment are shown in Figure 3.1 and Table 3.1. This vibration test is designed to be used as a practical and low cost diagnosis tool to examine the SOCs and SOHs of a LIB cell. Thus, all testing equipment are standard off-the-shelves equipment which are currently used in most industrial and academic work. Also, testing equipment are very compact and portable so that they could fit in a small size suitcase or a backpack for convenient transportation if needed.

The LIB cells used in this experiment are prismatic LIB cells manufactured by EnerDel. These are high capacity LIB cells which are mostly used as power sources in electric vehicles. The battery cell's dimension is $25 \times 17 \times 5$ cm, and its capacity is rated at 17.5 Ah which represents 1 C_{rate}. The C_{rate} represents how long a LIB can be completely charged or discharged, and the C_{rate} is determined by the total capacity of

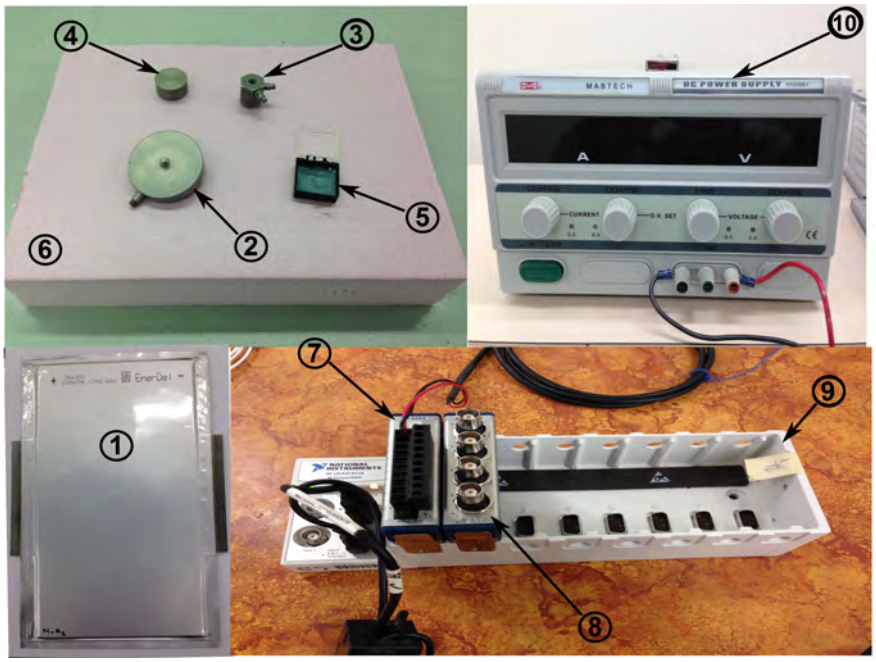

Figure 3.1: List of Vibration Test Equipment.

the LIB cell. At 1 C_{rate}, a LIB cell will be completely charged/discharged in 1 hour at a constant current of 17.5 A. However, it is recommended by the battery manufacturer to cycle the battery at 1/3 C_{rate} which is 5.8 A to obtain good measurement and to prolong the life of the battery cell.

3.1.1 Piezoelectric Actuator

For most active vibration-based testing, either acoustic or direct vibration excitation is used as a source to provide excitation input to the test object. The acoustic excitation is typically a speaker which can excite the test object by producing and transferring sound waves into the object. Most of the vibration excitation sources are based on piezoelectric technology. A piezoelectric actuator consists of a metal case and a core made of piezoelectric materials which is contained inside the case and attached to the bottom of the case; 2 exact same masses are attached on both sides of the core. The piezoelectric material is subjected to expand and contract under

Table 3.1: List of Testing Equipment.

Number	Name	Type	Comments
1	LIB Cells	EnerDel 17.5Ah	All cells have the same conditions
2	Piezoelectric Disk Actuator	PCB-712A02	Inertial Mass Actuator
3	Impedance Head	PCB-288D01	Combination of load cell and accelerometer
4	Mass	Stainless Steel, 200g	Provide stablility to the actuator and sensors
5	Wax	Petro Wax	Use as removable adhesive for accelerometer
6	Foam Block	High Density	Absorb excitation to eliminate the effect from the bottom surface.
7	Labview DAQ Output Module	NI-9263	Provide voltage to trigger actuator
8	Labview DAQ Input Module	NI-cRIO-9233	Receive load and acceleration signals from sensors
9	DAQ Chassis	NI-cDAQ-9128	Connect DAQ units to computer
10	DC Power Supply	MASTECH HY5020EX	Provide constant current charging of the battery cell

an applied voltage, and its amplitude correlates with the amplitude of voltage input. Vibration is generated as the attached masses moves with high velocity.

In this experiment, a piezoelectric disk actuator is used as an excitation input, Figures 3.2 and 3.3. A piezoelectric disk actuator operates on the same principle; however, the piezoelectric material in this case is a membrane whose outer diameter is attached to the inner diameter of the metal disk, and a small mass is attached at the center of the membrane to generate vibration as the tension and compression force occur on the membrane when a voltage is applied.

For most active vibration-based tests using piezoelectric actuators, the actuators are often attached on the objects by strong adhesive compound to provide stability to the test setup. However, that approach does not benefit the practical applications in battery testing because it will increase the setup time to attach and remove the actuator and sensors. Moreover, removing an adhered actuator and sensors from the surface of the battery cell may damage the cell. Therefore, the disk actuator

Figure 3.2: PCB-712A02 Piezoelectric Disk Actuator.

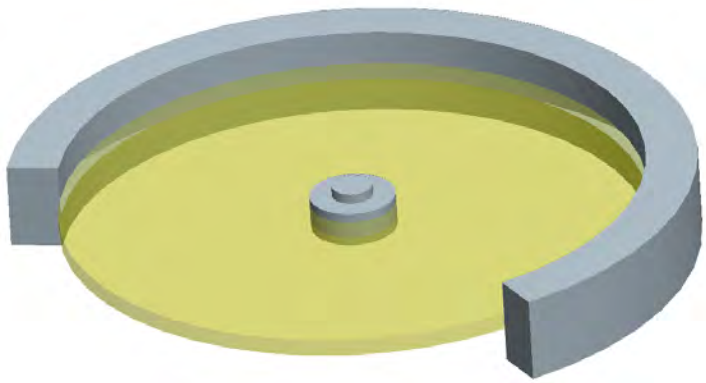

Figure 3.3: Operation of a Piezoelectric Disk Actuator.

brings several advantages to this battery testing technique when it can be applied without using strong adhesive. With an undisturbed testing environment, a mass can be attached on top of the disk actuator to provide stability to the test setup. Also, the weight of the mass can be changed to adjust the amplification of the excitation source. Also, an impedance head can be attached on the bottom of the disk actuator to create a solid structure which will provide efficient measurement. The PCB-712A02

disk actuator is used in this experiment, and its parameters are described in Table 3.2 below [15].

Table 3.2: PCB-712A02 Disk Actuator Characteristics.

Parameters	PCB-712A02
Voltage Input (Volts)	0 - 10
Effective Mass (grams)	12.14
Inertial Mass (grams)	200
Stiffness (kN/m)	401.5
Damping (Ns/m)	11.48

3.1.2 Impedance Head

Figure 3.4: PCB-288D01 Impedance Head.

The impedance head PCB-288D01 is shown in Figure 3.4 is used in this experiment. This is a mechanical impedance head which contains an accelerometer to obtain

the acceleration response from the test object as well as a load cell to measure the dynamic tension and compression force input. This impedance head is attached to the bottom of the disk actuator and mounted directly on the battery cell to maximize the efficiency in measuring the FRFs of the battery cell through the driving point measurements.

Table 3.3: PCB-288D01 Characteristics.

Performance	Units
Sensitivity (Acceleration) (±10%)	10.2 mV/(m/s^2)
Sensitivity (Force) (±10%)	22.4 mV/N
Measurement Range (Acceleration)	±490.5 m/s^2pk
Measurement Range (Force)	±222.4 N pk
Maximum Force	2224 N

3.2 Experimental Setup

Figure 3.5 shows the experimental setup for the vibration test of a LIB cell. An EnerDel LIB cell is placed on top of a high density foam block to minimize any interference response from the table. Two poles of the battery cell are connected to the Mastech DC power supply to charge the battery cell with constant current; the poles are also connected to the data acquisition (DAQ) unit to monitor actual battery cell's voltage. An impedance head which contains both a collocated accelerometer and a load cell is attached to the piezoelectric disk actuator and directly applied on the top surface of the LIB cell. The location of the driving point directly affects the FRFs of the battery cell because it determines how the structure will vibrate; therefore, driving point location is kept at the same spot, at 7.5 × 7.5cm from the corner of the cell, on every battery cell to maintain the consistent measurements. A thin layer of wax is applied on the interface between the impedance head and the battery cell's top surface to maintain surface contact and to maximize the input excitation by filling

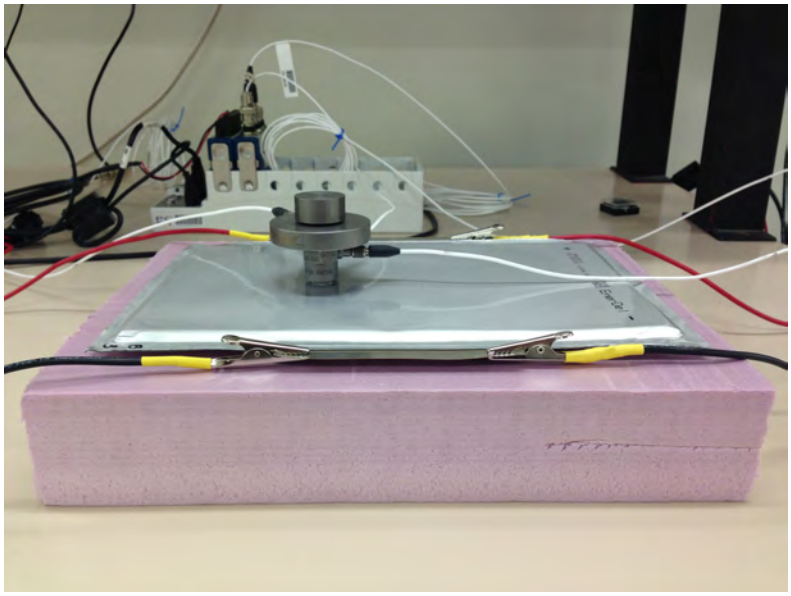

Figure 3.5: Vibration Test Setup.

the air gap caused by uneven surfaces. Also, a 200g mass is attached on top of the disk actuator to provide stability for the disk actuator and to provide amplification for the excitation input.

The test setup is contained inside a polycarbonate box, shows in Figure 3.6, to keep the testing environment from disturbance and to serve as hazardous containment in case of rupture or fire occurs when the battery cell fails or being overcharged during the experiment.

3.3 Experimental Procedure

The tests are designed to estimate the FRF of the battery at each 10% increment in the charge state. In order to measure the FRF at the exact SOC, the battery cell is put under constant current charge with 1/3 C_{rate}, and the charging time is determined by the total capacity of the cell (17.5 Ah), which is provided by the battery manufacturer. Based on the total capacity of this LIB cell, it will take 1 hour to completely charge the battery cell at 17.5A. Thus, at 1/3 C_{rate}, which is 5.8A, the

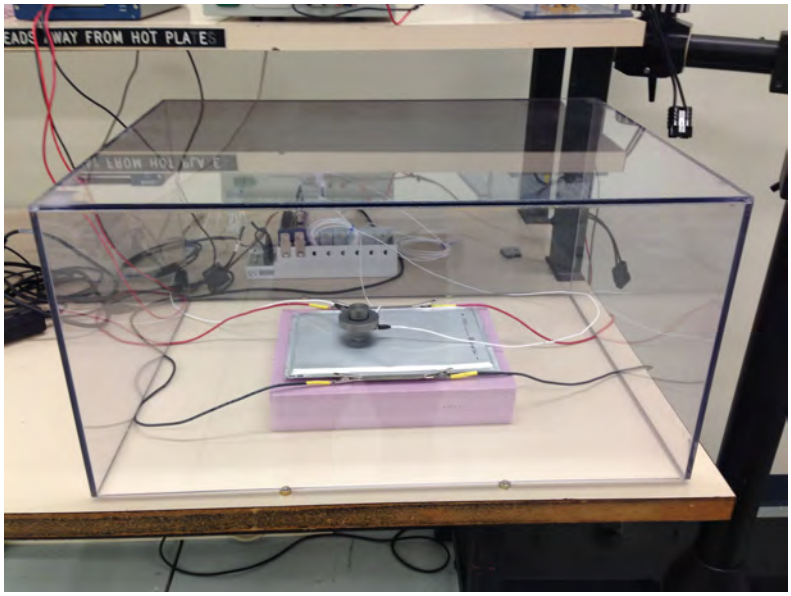

Figure 3.6: Vibration Test Setup in Controlled Environment.

total charging time will be 3 hours (180 minutes). It will take 18 minutes to charge the battery cell to each 10% SOC increment.

Figure 3.7 illustrates the testing sequence for a LIB cell. The SOCs of 100% and 0% are defined based on the maximum and cut-off voltages of the cell which are at 4.1V and 2.5V, respectively. The values of maximum and cut-off voltages are also provided by the battery manufacturer based on the design and configurations of this particular battery cell. Irreversible capacity losses, damage, or even total failure of the battery cell will occur when it is operated outside those limits.

In order to acquire an accurate measurement in the vibration test, the battery cell is required to reach steady state before any excitation can be applied because there is a certain time period after being charged or discharged during which Li-ions inside the cell are still in an excited state. This causes drift in charge and voltage. Therefore, the cell is permitted to relax for at least 6 hours before the FRF measurement can be taken to ensure there is minimum drifting effect so that it does not affect the test results. There are two types of variables which affect the SOCs and SOHs of a LIB cell; they are internal variables such as physical and material properties of the

components inside the cell, and external variables such as rate of charge/discharge, temperature, and storage time. In order to measure the SOC of a battery cell through changes in physical properties of electrodes, the other variables need to keep constant to maintain the consistency of the measurements. Therefore, the external variables are kept the same at 22°C and 1/3 C_{rate} for every battery test.

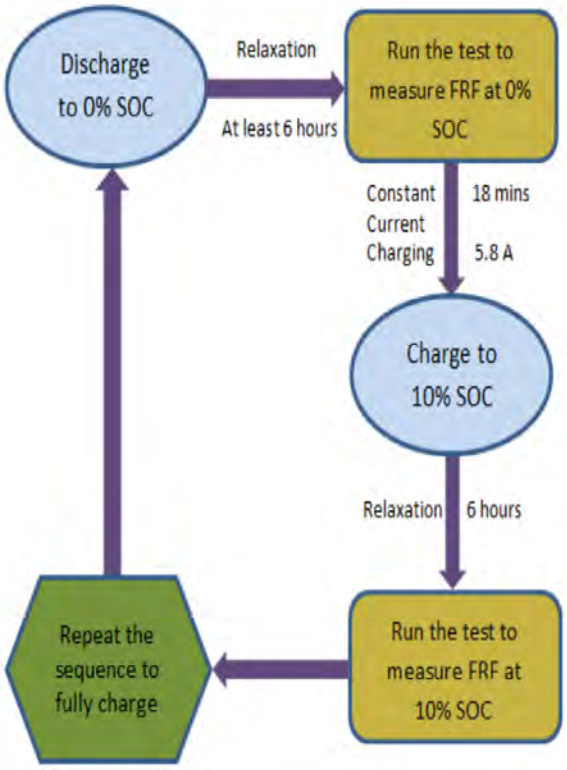

Figure 3.7: Vibration Testing Sequence.

The LIB cell is discharged to 2.5V at which it is considered at 0% SOC. After the relaxation period of 6 hours, the LIB cell at 0% SOC has reached the steady state. A vibration test is applied to obtain FRF at 0% SOC. Then, the LIB cell is charged for 18 minutes at 5.8A to reach 10% SOC. Another vibration test is applied to obtain FRF at 10% SOC after the LIB cell is let to relax for 6 hours. This sequence is

repeated until the LIB cell is charged to 180 minutes; at this state, it is considered at 100% SOC.

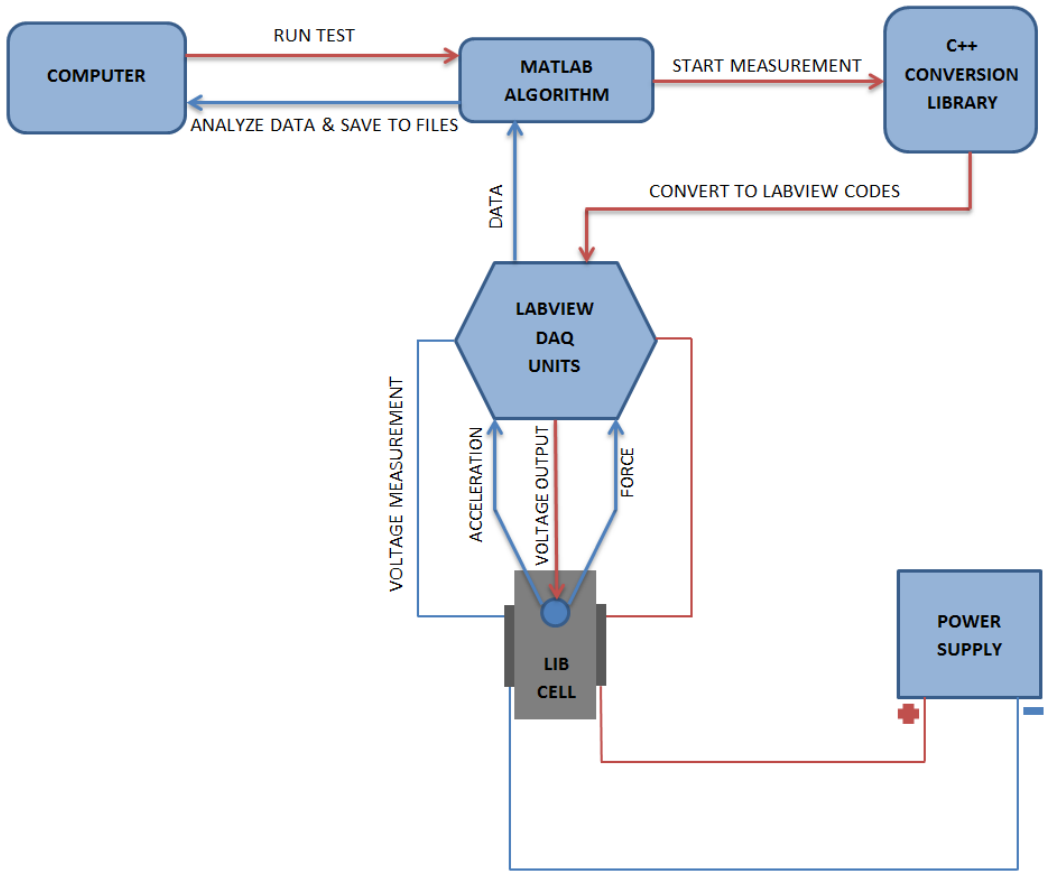

Figure 3.8: Vibration Test Schematic.

A vibration test is described in Figure 3.8. An algorithm is generated using Matlab to start the driving point measurement at every 10% SOC increment. A conversion library, which is an application package provided by Matlab, is used to communicate between Matlab algorithm and LabVIEW DAQ units. The test parameters are put in Matlab algorithm. As the test starts, Matlab program sends testing information to DAQ units through conversion library. Input and output DAQ units receive information from the program and send signals to trigger the actuator to apply an excitation to the LIB cell. The load cell and accelerometer then measure the force input and

acceleration response from the LIB, respectively. The measurement data is sent to Matlab to be analyzed and saved into files.

Table 3.4: Parameters for estimating FRF of the LIB cell.

Parameters	Value/Type
Sweep Frequency	0-5000 Hz
Sampling Frequency	50000 samples/sec
Duration	4 sec
Signal Filter	Anti-aliasing
Window	Tukey

A sine sweep with the frequency from 0 to 5000 Hz and with the duration of 4 seconds is used as an excitation on the LIB cell. The data obtained from the test is the force input and the acceleration output in the time domain. To estimate the FRF of the LIB cell, a Matlab program is generated to analyze the experiment data. The program processes the data by passing them through an anti-aliasing filter to eliminate overlapped signal; then, a Tukey window is applied to the data to minimize spectral leakage before it is converted to frequency domain using Fast Fourier Transform (FFT) function in Matlab. Finally, FRF from the data is produced using H1 estimator to minimize the noise output. The parameters used for estimating the FRFs are summarized in Table 3.4.

3.4 Experimental Results

The FRF magnitude of the LIB cell at 10% SOC is shown in Figure 3.9. The highly damped resonances observed from the FRF correlate with the components' properties within the battery cell. The electrolyte inside the battery cell is either liquid or gel which can result in a highly damped structure. This FRF can serve as the SOC and SOH signature of the LIB cell at 10% SOC because it reflects the

conditions of the LIB cell's structure at this state. Therefore, this FRF can be used as a reference in determining the SOC at 10%.

The coherence is also shown in Figure 3.9. The coherence represents the causality of the system; as the coherence value reaches 1, the system is causal. It means the total response output measured is linearly correlated with the input power. The coherence value in this measurement is equal to 1 after approximately 250 Hz. This result suggests that in the frequency range from 250 to 5000 Hz; thus, there is a good signal to noise ratio. Therefore, the measurement is good and reliable.

The FRFs obtained from each 10% increment SOC are shown together on one plot, Figure 3.10 & 3.11, to illustrate how the FRF changes when the LIB cell increases in SOC. As the LIB cell is charged, the FRF of later SOC slightly shifts to the right of the previous one. This indicates that the LIB cell responds at higher frequencies as it reaches a higher SOC. Except the last two SOCs at 90 and 100%, all other FRFs have similar spacing between them, which correlates with the increment changes in the LIB SOC. During the test, the cell was charged with constant current and the same time for every SOC. There is nearly equal amount of Li-ions was transported from one electrode to another at every SOC. It causes the properties of electrodes to change at the same rate. In other words, there is a nearly linear relationship between the cell SOC and the physical properties of the electrodes inside the LIB cell.

3.5 Experimental Verification

3.5.1 Sensitivity Verification

The driving point measurements are used in this experiment to obtain the FRFs of the LIB cells. However, the driving point measurement is dependent on the applied location of the test object and the amplitude of the input excitations. The response from the location on the test object, which is farther away from the driving point, will be less than the one that is closer to the driving point. Therefore, the sensitivity

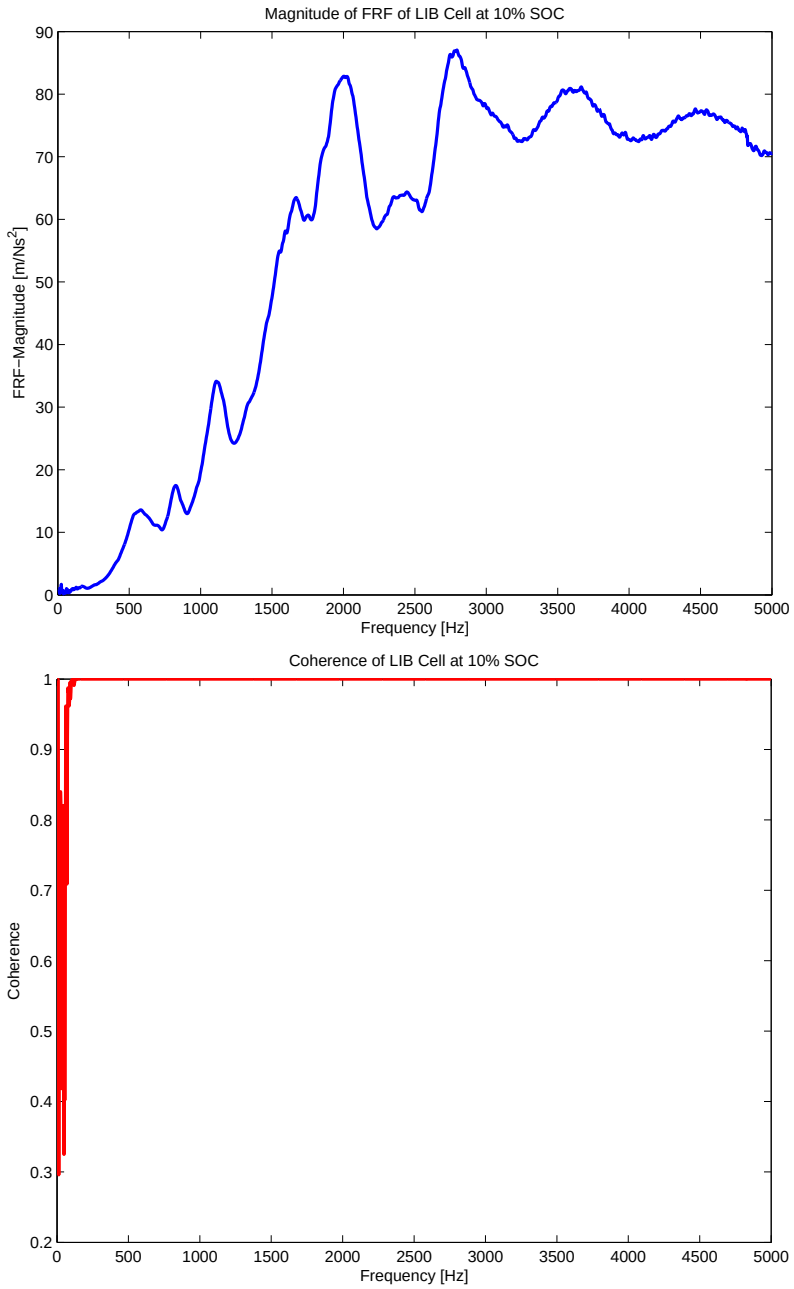

Figure 3.9: FRF Magnitude and Coherence of a LIB Cell at 10% SOC.

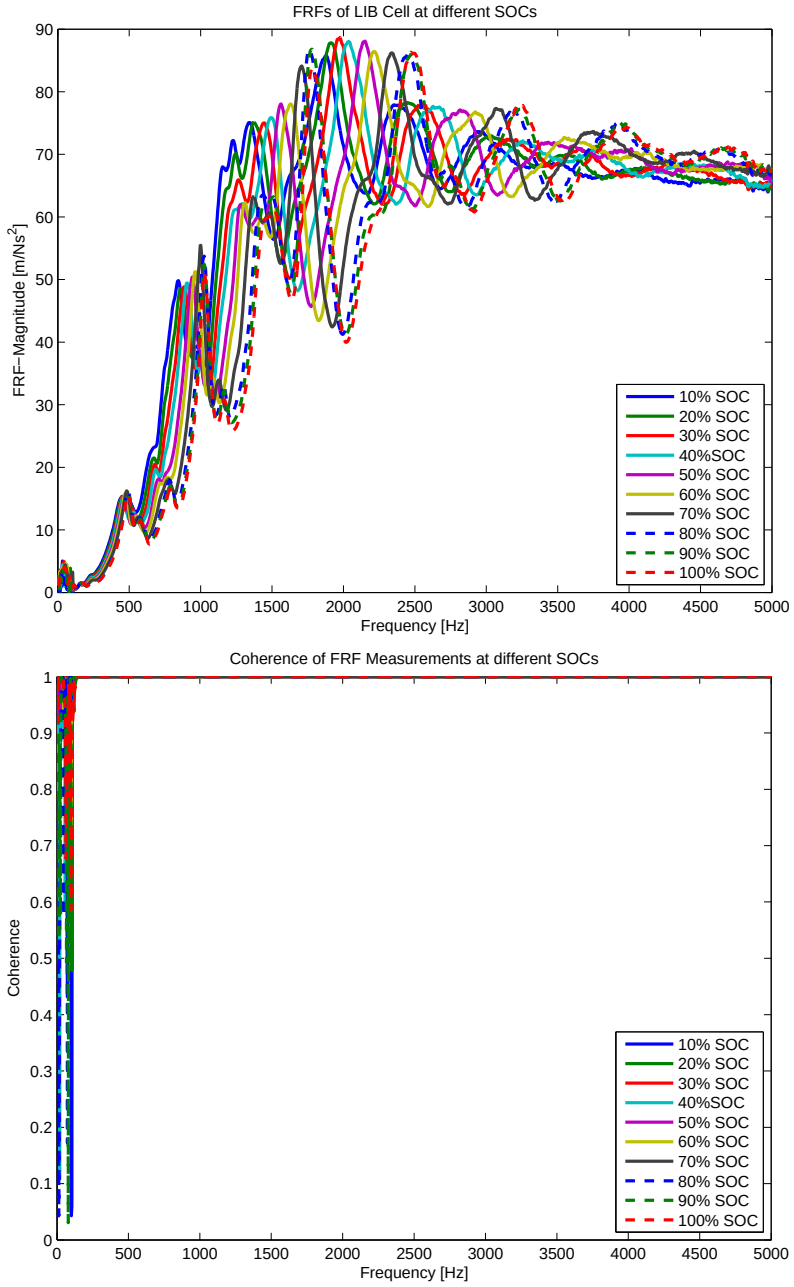

Figure 3.10: FRFs Magnitude and Coherence of A LIB Cell at Different SOCs.

verification is performed to ensure the driving point measurement in this experiment is able to reflect the condition of the whole LIB cell.

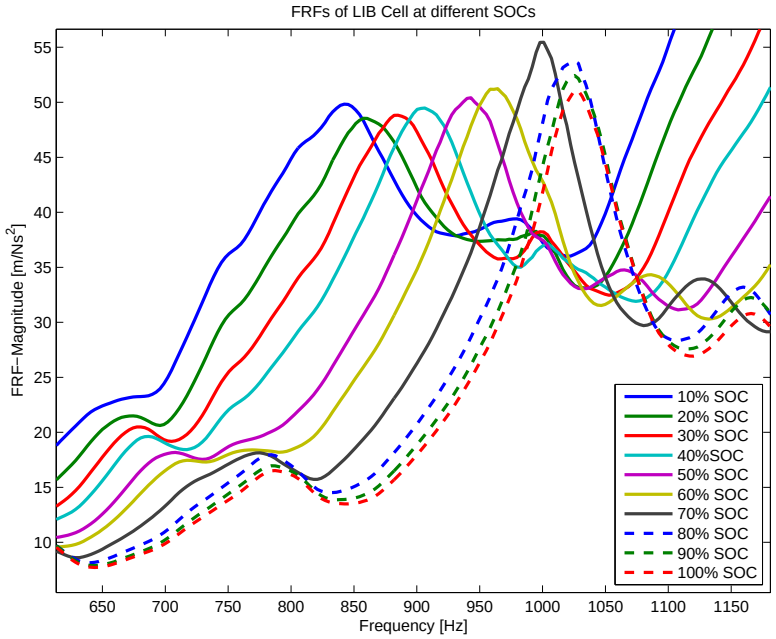

Figure 3.11: Magnification of FRFs at Different SOCs.

Figure 3.12: A Polycarbonate Plate Used For Sensitivity Verification.

Figure 3.12 shows a polycarbonate plate, which has the same dimension as the LIB cell, is used in this study. The driving point measurements are applied to the

undamaged polycarbonate plate to obtain its FRF. Then, a small change is created at the farthest corner from the driving point on the plate to introduce a change to the plate's structure. The FRF obtained from the damaged plate will be used to compare with the undamaged plate to verify the sensitivity of the experiment.

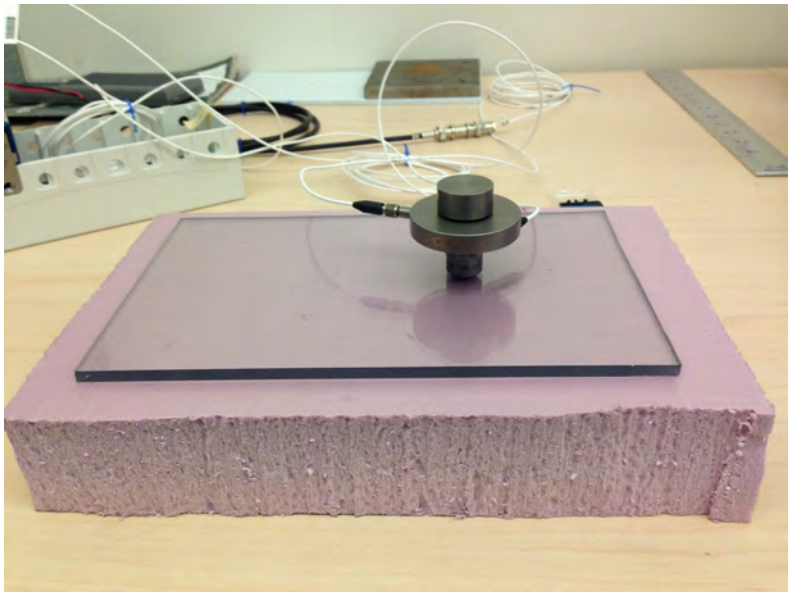

Figure 3.13: Driving Point Measurement on Polycarbonate Plate.

The setup of the sensitivity test is demonstrated in Figure 3.13. The sensitivity verification setup is identical to the vibration test stup of the LIB cell. The driving point measurement is taken twice on the same polycarbonate plate at different time to compare the FRFs of the unchanged polycarbonate plate.

The FRFs obtained from 2 different driving point measurements of the same polycarbonate plate are shown in Figure 3.14. The result shows that the FRFs are identical as the polycarbonate plate is unchanged in its structure.

A small change in the polycarbonate plate's structure is created by drilling a hole with the dimension of 1/8 inches in diameter and 1/16 inches in depth on the polycarbonate plate. The drilling on the polycarbonate plate is done without disturbing the test setup to ensure it is the only change in this experiment. Another driving point measurement is taken to obtain the FRF of the damaged polycarbonate plate.

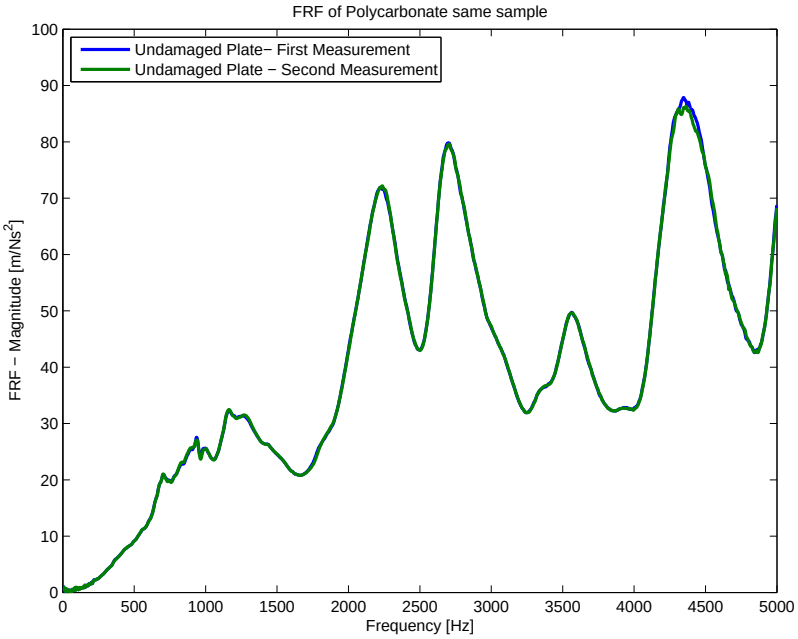

Figure 3.14: FRFs From Driving Point Measurement for Polycarbonate Plate.

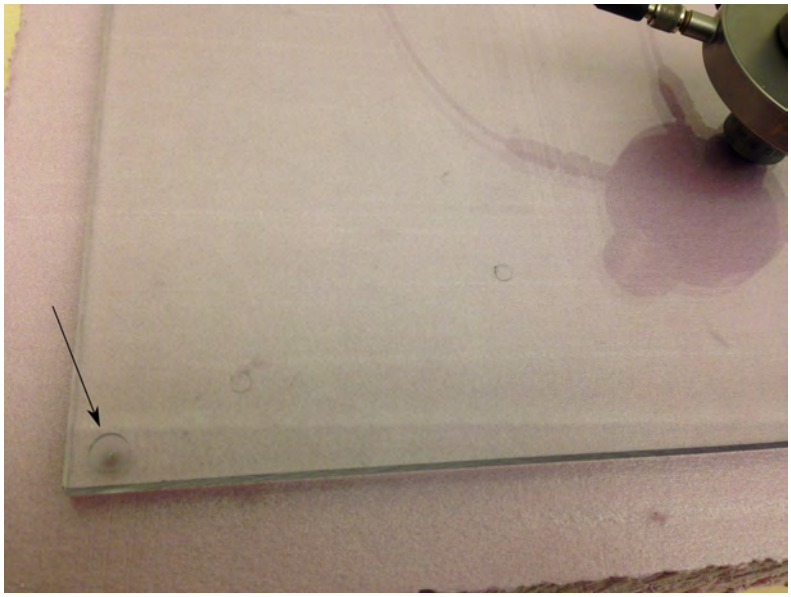

Figure 3.15: A Damage Introduced on Polycarbonate Plate.

The FRF obtained from the damaged plate will be used to compare with the FRF of the undamaged one.

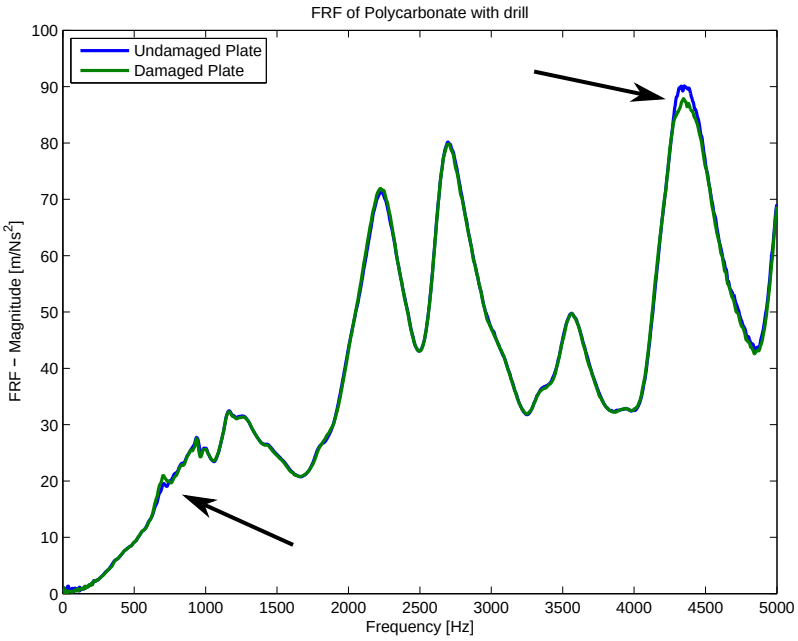

Figure 3.16: FRFs Before and After Damage on Polycarbonate Plate.

The FRFs of the polycarbonate plate before and after it is drilled are shown in Figure 3.16. The arrows indicate the differences in the FRFs of the polycarbonate plate before and after the plate is changed in its structure.

The results from this sensitivity study verify that this testing technique can measure the differences in FRFs of the undamaged and damaged polycarbonate plate at the farthest point from the driving point. Thus, the vibration test can reflect the structural change of the whole battery cell.

3.5.2 Repeatability Verification

In order to verify the results from the vibration tests, a different LIB cell is discharged to 0% SOC. Then, it is charged for 90 minutes with constant current at 1/3 C_{rate}. After the battery cell has relaxed for 6 hours, a vibration test is taken to measure the FRF and estimate its current SOC. Also, the true SOC is calculated using the known charging current and the time used to charge the battery cell. The true SOC will be compare with the SOC measured from the vibration test.

Equation (2.3) is used to calculate the true SOC of the battery cell.

$$SOC = \frac{I \times t}{Q} \times 100 = \frac{5.8A \times 1.5h}{17.5Ah} \times 100 = 50\%. \tag{3.1}$$

In Figure 3.17, the FRF of the new LIB cell is plotted on the same plot with the previous FRFs plot to examine if the vibration test can be repeated on other LIB cells which have similar specifications. The dashed red curve shown on the plot is the FRF of the new LIB cell which is charged to 50% SOC. The result from Figure 3.17 indicates that the FRF of new LIB cell is nearly matching the previous battery cell's FRF at 50%. There are differences in amplitude of the resonant frequencies of the 2 battery cells. The small differences in the FRFs are caused when the actuator and sensors are removed from one battery cell and applied to another. The small changes in the initial conditions of the measurement such as location, wax layer, and the compression force used to attach the actuator onto the battery cell's surface will

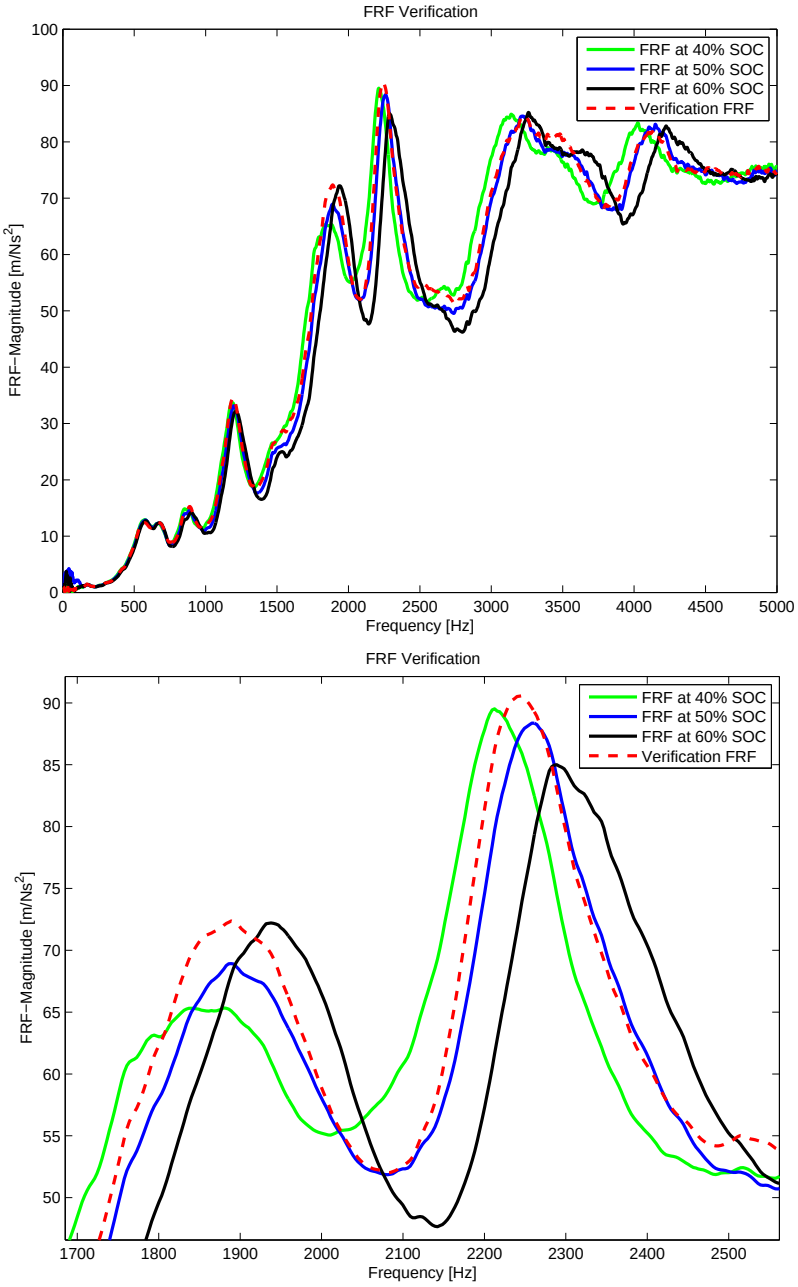

Figure 3.17: Compare FRFs of 2 Different LIB Cells at 50% SOC.

affect the measurement. However, the differences are small, and there is no shifting in resonant frequencies of the 2 battery cells. Therefore, the vibration test is reliable and repeatable.

4. ELECTRODES MECHANICAL PROPERTIES MEASUREMENT AND THICKNESS CHANGE ESTIMATION

It is essential to develop a dynamics model for a LIB cell to confirm the vibration test results. The model is also used to investigate the effect of an electrode's properties changes to the SOCs and SOHs of a battery cell. The development of a LIB cell's dynamics model requires to obtain the mechanical properties of the electrodes inside the battery cell to provide initial values for the model's parameters. However, it is very difficult to measure the mechanical properties of the electrodes inside an active LIB cell. Because active electrode materials are very reactive after they are activated, it is required a sophisticated controlled environment to be able to perform the direct measurements of the electrodes inside an active cell. Once an active battery cell is open, the electrodes will react to the moister in the open air and form oxidation on their surfaces. That oxidation will result in the degradation and failure of the electrodes' materials. Also, the electrodes inside the battery cell are soaked with electrolytes; and the electrolytes will evaporate quickly once it is released. Thus, measuring the mechanical properties of the active electrodes is not practical. The alternative for this problem is measuring the mechanical properties of the non-active electrodes; then, a mathematical model is used to estimate the properties changes of the active electrodes at different SOCs using the non-active electrodes' mechanical properties. The only difference between a non-active and an active electrode is the swelling effect when an electrode goes through the wetting process. When a non-active electrode is activated by wetting it with electrolyte, its thickness will increase as it absorbs electrolyte. Thus, the properties of the active electrodes inside the LIB cell can be obtained by incorporating the swelling factor into the measure properties of the non-active electrodes. The non-active electrodes are measured using the Dynamics

Mechanical Analyzer (DMA), and a mathematical model will be used to estimate the changes in thickness of an electrode at different SOCs.

4.1 Electrodes' Mechanical Properties Measurement using Dynamics Mechanical Analyzer

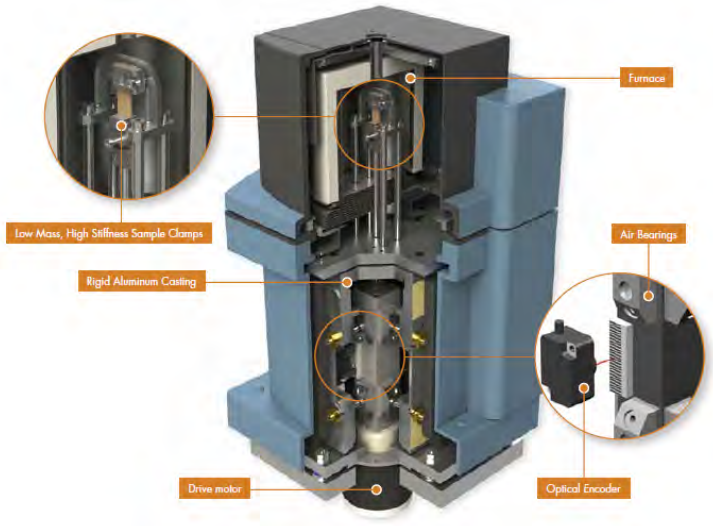

Figure 4.1: Dynamics Mechanical Analyzer.

The DMA is an automatic measuring device used to measure the mechanical properties of a wide range of materials including viscoelastic materials. A DMA system includes a sample chamber which is capable of precise temperature control, a heated vapor-transfer line to maintain chamber temperature, and a control system to monitor and control humidity and temperature of the sample chamber. One of the advantages of the DMA is the ability to measure samples using non-contact linear drive technology to maximize precision control of stress. Also, air bearings reduce friction support. Optical encoder technology is used to measure strain to obtain high accuracy and resolution. Some relevant specifications of the DMA are summarized in Table 4.1.

Table 4.1: Dynamics Mechanical Analyzer Specifications.

Modes of Deformation	Dual/Single Cantilever, 3-Point Bend, Shear Sandwich, Compression, Tension, Submersible Clamps
Modes of Operation	Multi-Frequency, Multi-Stress/Strain, Creep/Stress Relaxation, Controlled Force/Strain, Isostrain
Max/Min Force	18/0.0001 N
Temperature Range	-150 - 600^oC
Frequency Range	0.01 - 200 Hz
Modulus Range	10^3- 3×10^{12} Pa

The components are required to measure are the cover layer, single-side cathode, double-side cathode, and double-size anode. To measure the mechanical properties of those components, they are disassebled from the battery cell and cut into small specimens with a dimension of 1×5cm. A micrometer is used to measure the thickness of the electrodes and cover layer. Each specimen is weighted to calculate its density. Then, the DMA is used to measure the mechanical properties of each specimen. The measured dimension and thickness of each sample is entered to the DMA system to calculate the stress and strain of the sample.

Tension test with controlled force is used to measure the properties of the components' samples. Figure 4.2 shows a cathode sample is put on the clamp in the testing chamber. The preload force is set at 4 Newtons. The preload force is held until the temperature inside the chamber reaches29^oC. The preload time provides the steady state condition inside the DMA chamber and ensures the sample is in tension before the measurement starts. An increment of 2 N is applied to the sample every 5 minutes until it reaches maximum load of 18N. The DMA measures the strain of the sample and calculate its stress based on the force input and the dimensions of the

sample. Therefore, a stress/strain curve of the sample can be constructed from the measurement.

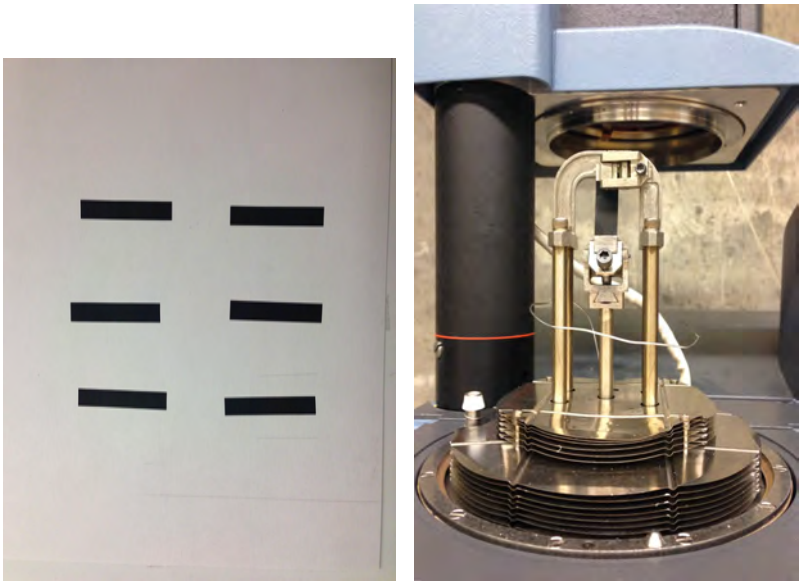

(a) (b)

Figure 4.2: (a) Electrode Samples. (b) DMA Testing Setup.

Stress vs Strain plots of different samples are shown in Figure 4.3. The Elastic modulus of a sample can be obtained by contructing a slope on the linear region of the stress vs strain curve. The measured mechanical properties of different components of a non-active LIB cell are summarized in Table 4.2.

Table 4.2: Measured Properties of an Inactive LIB Cell Components.

Components	Dimension (cm)	Electrode Material Thickness (cm)	Density (g/cm^3)	Elastic Modulus (MPa)
Cover Layer	$14.5 \times 23.5 \times 0.016$	NA	1.6875	4151
Single-side Cathode	$14.5 \times 23.5 \times 0.010$	7×10^{-3}	2.7900	8342
Double-side Cathode	$14.5 \times 23.5 \times 0.015$	14×10^{-3}	1.8846	3137
Double-side Anode	$14.5 \times 23.5 \times 0.013$	12×10^{-3}	2.8293	3442

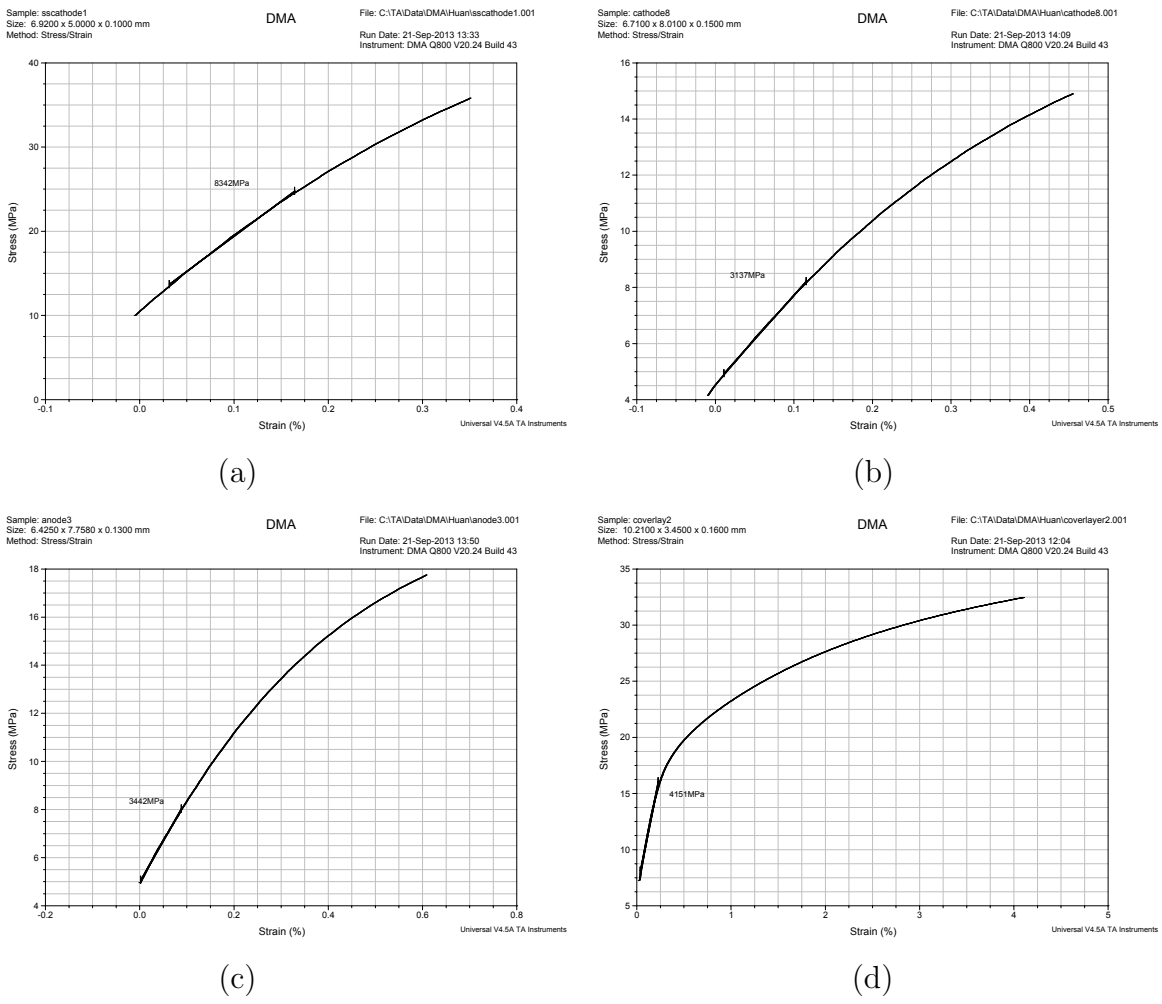

Figure 4.3: Stress vs Strain Curves of (a) Single-side Coated Cathode. (b) Double-side Coated Cathode. (c) Double-side Coated Anode. (d) Cover Layer.

4.2 Electrodes' Thickness Change Estimation

The electrodes' thickness is changed during charging and discharging cycle. The changes occur when Li-ions are removed from and inserted in the electrodes' structures. The thickness changes will create contraction and expansion in the electrodes materials. Therefore, cycling a battery cell will create cyclic loads on its electrodes, and it can cause fatigue on the electrodes and destroy the battery cell. Also, the electrochemical intercalation process on the electrodes occurs during cycle creates ion concentration in the electrodes' materials; thus, the concentration of Li-ions will induce mechanical stress on the electrodes. When the stress exceeds the limits of electrodes' materials, permanent deformation or fractures will occur in the electrodes' materials which lead to irreversible capacity loss or failure of a LIB cell. Thus, to be able to estimate the changes of electrodes' thickness inside the battery cell during charge or discharge will help to determine the stress on the electrodes inside the battery cell at different SOCs. Moreover, the estimated thickness changes can be used as inputs for a dynamics model to diagnose health of a LIB cell.

A mathematical model is developed by Fu et al [10] to estimate the thickness change in cathode and anode as a function of ion concentration and the SOC of the LIB cell. By using the mechanical properties of the electrodes obtained from DMA measurements in the previous section, the thickness changes of the electrodes at different SOCs can be estimated by the dynamics model of the battery cell.

Table 4.3 lists the mechanical properties of the lectrodes measured from the DMA measurement, and the parameters of electrodes' thickness changes obtained from electrochemical properties of the similar type LIB by Smith and Wang [16].

The change in radius of electrode particle can be expressed as

$$\triangle R_s = \frac{1}{3}\bar{c_s} \cdot \Omega \cdot R_{s0}. \tag{4.1}$$

The relationship between the change in volume of an electrode and the one of an electrode particle can be expressed as

Table 4.3: Estimation Parameters. [16]

Parameter	Anode	Cathode	Units
Initial Thickness h_o	6×10^{-3}	7×10^{-3}	cm
Particle Radius, R_{s0}	10^{-4}	10^{-4}	cm
Active Material Volume Faction, ε_s	0.58	0.50	
Elastic Modulus, E	3442	3137	MPa
Poisson's Ration, υ	0.3	0.3	
Fractional Expansivity, ω	0.08	0.065	
Stoichiometry at 0%,$x_{0\%}, y_{0\%}$	0.126	0.936	
Stoichiometry at 100%, $x_{100\%}, y_{100\%}$	0.676	0.442	

$$\frac{V}{V_0} = \left(\frac{V_s}{V_{s0}}\right),^g \tag{4.2}$$

where V and V_0 are the volumes of the electrodes with and without expansion by lithiation, respectively. $V_s$and $V_{s0}$are volumes of electrode particles with and without expansion by lithiation, respectively. And g is the swelling coefficient; in this case, assume the total volume changes of the electrodes are from the volume changes of electrode particles; so, g is equal to 1. Therefore, Equation (4.2) can be linearized as

$$\triangle V = 3V_0 \frac{\triangle R_s}{R_{s0}}. \tag{4.3}$$

Because the area of an electrode is a constant as the material cannot expand beyong the coated area, the volume change occurs through the thickness change. The Equation (4.3) can be rewritten as:

$$\triangle h = 3h_0 \frac{\triangle R_s}{R_{s0}}, \tag{4.4}$$

where h_0 is the initial thickness of electrode without expansion by lithiation, and $\triangle$h is the thickness change caused by lithiation. Subtitute Equation(4.1) into

Equation(4.4) will give the thickness change of electrode as a function of average ion concentration.

$$\triangle h = \Omega \cdot h_{0.}\bar{c_s}. \tag{4.5}$$

The average ion concentration can be obtained from the SOC of the battery cell and Stoichiometric numbers of negative and positive electrodes. So, there is difference in the average ion concentration of the cathode and the anode. They can be expressed as:

$$\bar{c_s^-} = (x_{0\%} + (x_{100\%} - x_{0\%}) \cdot SOC) \cdot c_{s,max}^-. \tag{4.6}$$

$$\bar{c_s^+} = (y_{0\%} + (y_{100\%} - y_{0\%}) \cdot SOC) \cdot c_{s,max}^+, \tag{4.7}$$

where - and + represent anode and cathode, respectively. Also, x and y are Stoichiometric number of anode and cathode, respectively.

Substitute Equation(4.6) & (4.7) into Equation(4.5), the thickness change becomes

$$\triangle h^- = \left(\Omega^- \cdot h_0^- \cdot c_{s,max}^- \cdot x_{0\%}\right) + \left(\Omega^- \cdot h_0^- \cdot c_{s,max}^- \cdot (x_{100\%} - x_{0\%})\right) \cdot SOC. \tag{4.8}$$

$$\triangle h^+ = \left(\Omega^+ \cdot h_0^+ \cdot c_{s,max}^+ \cdot y_{0\%}\right) + \left(\Omega^+ \cdot h_0^+ \cdot c_{s,max}^+ \cdot (y_{100\%} - y_{0\%})\right) \cdot SOC. \tag{4.9}$$

Equation(4.8) & (4.9) clearly indicate how the thickness of the anode and the cathode will change at different SOCs. The Stoichiometric number of anode at fully charged is greater than the one at fully discharge. So, the quantity of $(\mathrm{x}_{100\%} - \mathrm{x}_{0\%})$ is positive. On the other hand, Stoichiometric number of cathode at fully charged is less than the one at fully discharged; so, $\mathrm{y}_{100\%} - \mathrm{y}_{0\%}$ is a negative number. Therefore,

as the SOC increases, thickness of the anode will increase, and thickness of cathode will decrease. This correlates with the actual operation of the LIB cell because during charging cycle, Li-ions are removed from cathode and inserted to anode. Thus, cathode' thickness will decreases, and anode's thickness will increase.

The maximum ion concentration of an electrode can be obtained when the thickness of an electrode reaches maximum value. Therefore, maximum ion concentration of anode and cathode can be calculated as

$$c_{s,max}^{-} = \frac{Q}{(x_{100\%} - x_{0\%}) \cdot h_{max}^{-} \cdot \varepsilon_s^{-} \cdot A \cdot F \cdot N}. \tag{4.10}$$

$$c_{s,max}^{+} = \frac{Q}{(y_{0\%} - y_{100\%}) \cdot h_{max}^{+} \cdot \varepsilon_s^{+} \cdot A \cdot F \cdot N}, \tag{4.11}$$

where Q is the total capacity of the battery cell, h_{max} is the maximum thickness of an electrode after being lithiated, ε_s is the active material volume fraction which can be obtained from Table4.3, A is the area of an electrode, F is the Faraday constant, and N is the number of single electrode material layers.

When the electrode is fully lithiated, the volume change is maximum, and it can be expressed as

$$\frac{V_{s,max}}{V_{s0}} = \left(\frac{R_{s,max}}{R_{s0}}\right)^3 = 1 + \omega, \tag{4.12}$$

where $\omega$is the factional expansivity of electrode material. Therefore, the maximum thickness change can be obtained as

$$h_{max} = (1 + \omega) \cdot h_0. \tag{4.13}$$

Also, the change of electrode particles radius will become maximum when the average ion concentration is at its maximum value.

$$\triangle R_{s,max} = \frac{1}{3} \bar{c}_{s,max} \cdot \Omega \cdot R_{s0}. \tag{4.14}$$

Therefore, the theoretical partial molar volume of anode and cathode can be obtained by substituting Equation(4.14) into Equation(4.12)

$$\Omega^{-} = \frac{3}{c^{-}_{s,max}} \left[\left(1 + \omega^{-}\right)^{\frac{1}{3}} - 1 \right]. \tag{4.15}$$

$$\Omega^{+} = \frac{3}{c^{+}_{s,max}} \left[\left(1 + \omega^{+}\right)^{\frac{1}{3}} - 1 \right]. \tag{4.16}$$

Substitute Equation (4.10), (4.13), (4.15) into Equation(4.8); and substitute Equation (4.11), (4.13), (4.16) into Equation(4.9), thickness change an electrode becomes a function of the SOC only. Thus, the thickness of each electrode can be obtained at different SOC.

The mechanical properties and the thickness changes of the electrodes obtained from this section will be used as variables in the analytical model of the battery cell. This model is very helpful in studying the effect of mechanical properties and thickness changes in electrodes to the changes of the FRFs. Comparing the FRF results from the model and the ones from the vibration tests, the information about the effect of physical properties changes in the electrodes to the SOCs and SOHs of the LIB cell will be revealed.

5. ANALYTICAL MODEL OF A LITHIUM-ION BATTERY CELL

There are many factors that affect the components' material properties inside a LIB cell which directly affect the SOCs and SOHs of the battery cell. A vibration test can reveal the differences in FRF of a LIB cell when a change occurs within the battery cell's structure. However, results from vibration tests alone do not provide enough information to identify the source which causes changes in FRFs. By using the battery cell's structure and operation to construct the analytical model of the LIB cell, the relationship between the changes in components' properties inside a LIB cell and the battery cell's SOCs and SOHs can be obtained. Moreover, the combination of the vibration test results and the analytical model of the battery cell can be used as a diagnostic tool to identify the sources of changes in the components' properties of a battery cell. This diagnostic tool can also identify the souces which cause the degradation in SOCs and SOHs of a LIB cell.

A LIB cell can be treated as a dynamics system with mass, stiffness, and damping. In order to model the battery cell as a dynamics system, it is required to obtain the mass and stiffness of the battery cell. Therefore, finite element method will be used to obtain the mass and stiffness of the battery cell using the physical properties of the battery cell's components.

5.1 Finite Element Method

A LIB cell is broken into a system of several layers of cover, anode, and cathode. Each layer is splitted into several elements which are connected together by nodes. Every node in one layer is connected to the one in the other layer by springs. Each element is considered as a Bernoulli's beam. Thus, mass and stiffness matrices of each element can be obtained by applying Bernoulli's Beam equations.

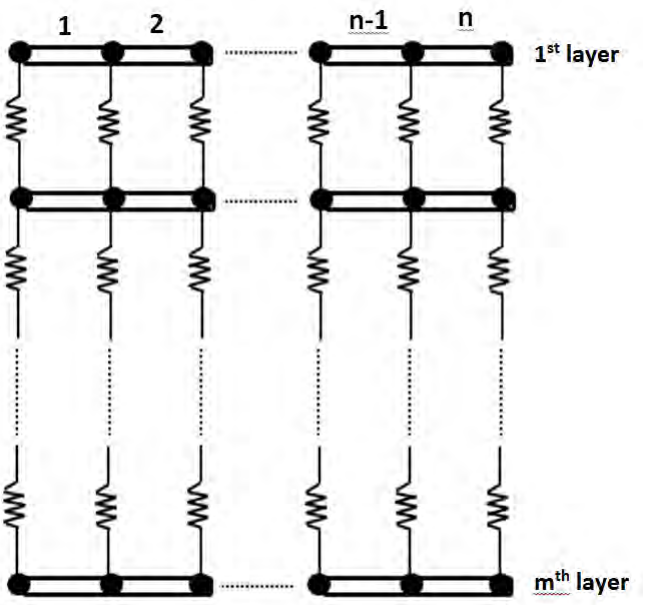

Figure 5.1: Finite Element Structure of a LIB Cell.

Figure 5.1 shows the structure of a LIB cell as a system of elements which are connected together by nodes and springs.

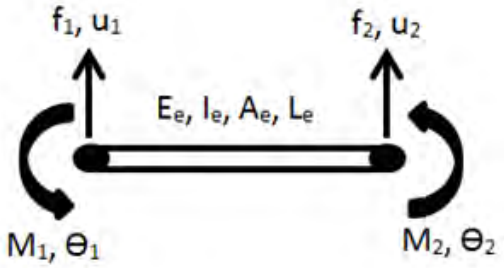

Figure 5.2: Free Body Diagram of a Beam Element.

The free body diagram (FBD) of an element is shown in Figure5.2. The deformation of this 4 degree of freedom beam can be described as a function of the end displacements

$$u(x,t) = \sum_{n=1}^{4} \psi_n(x) v_n(t), \tag{5.1}$$

Where u(x, t)is the deformation function of the beam, ν_{n}(t) are the end displacement functions, andψ_{n}(x) are the shape functions and they are expressed as follow:

$$\psi_1(x) = 1 - 3\left(\frac{x}{L}\right)^2 + 2\left(\frac{2}{L}\right)^3. \tag{5.2}$$

$$\psi_2(x) = x - 2\frac{x}{L}^2 + \frac{x^3}{L^2}. \tag{5.3}$$

$$\psi_1(x) = 3\left(\frac{x}{L}\right)^2 - 2\left(\frac{2}{L}\right)^3. \tag{5.4}$$

$$\psi_1(x) = \frac{x}{L^2}^3 - \frac{x}{L}^2. \tag{5.5}$$

For bending, the strain energy relates to the curvature κ, where it is expressed as:

$$\kappa = \frac{\partial^2 u(x,t)}{\partial x^2} = \sum_{n=1}^{4} \frac{\partial^2}{\partial x^2} \psi_n(x) \cdot v_n(t) = \sum_{n=1}^{4} \psi_n''(x) \cdot v_n(t). \tag{5.6}$$

The strain energy for pure bending can be obtained from the expression below:

$$V = \frac{1}{2} \int_0^L EI(\kappa)^2 dx. \tag{5.7}$$

Substitute the curvature from Equation(5.6) into Equation(5.7)

$$V = \frac{1}{2} \int_0^L EI \left(\sum_{n=1}^{4} \psi_n''(x) \cdot v_n(t) \right)^2 dx. \tag{5.8}$$

The stiffness coefficients can be expressed as:

$$K_{ij} = \frac{\partial}{\partial v_i} \frac{\partial}{\partial v_j} \frac{1}{2} \int_0^L EI \left(\sum_{n=1}^{4} \psi_n''(x) \cdot v_n(t) \right)^2 dx. \tag{5.9}$$

$$K_{ij} = \int_0^L E \cdot I \cdot \psi_i^{''}(x) \cdot \psi_j^{''}(x) dx. \tag{5.10}$$

Take the second derivative of the shape functions, it will yield the components of the element's stiffness matrix

$$[K_e] = \frac{E_e I_e}{L_e^3} \begin{bmatrix} 12 & 6L_e & -12 & 6L_e \\ 6L_e & 4L_e^2 & -6L_e & 2L_e^2 \\ -12 & -6L_e & 12 & -6Le \\ 6L_e & 2L_e^2 & -6L_e & 4L_e^2 \end{bmatrix}. \tag{5.11}$$

To find the element's mass matrix, start with velocity equation

$$\dot{u}(x) = \sum_{n=1}^{4} \psi_n(x) \cdot \dot{v}_n. \tag{5.12}$$

The kinetic energy of the neutral axis can be expressed as:

$$T = \frac{1}{2} \int_0^L \rho \cdot A \cdot (\dot{u}(x))^2 \, dx. \tag{5.13}$$

$$T = \frac{1}{2} \int_0^L \rho \cdot A \cdot \left(\sum_{n=1}^{4} \psi_n(x) \cdot \dot{v}_n \right)^2 dx. \tag{5.14}$$

So, the mass matrix coefficients can be obtained by

$$M_{ij} = \frac{\partial}{\partial \dot{v}_i} \frac{\partial}{\partial \dot{v}_j} \frac{1}{2} \int_0^L \rho \cdot A \cdot \left(\sum_{n=1}^{4} \psi_n(x) \cdot \dot{v}_n \right)^2 dx. \tag{5.15}$$

$$M_{ij} = \int_0^L \rho \cdot A \cdot \psi_i(x) \cdot \psi_j(x) dx. \tag{5.16}$$

Then, the mass matrix can be constructed as

$$[M_e] = \frac{\rho_e L_e}{420} \begin{bmatrix} 156 & 22L_e & 54 & -13L_e \\ 22L_e & 4L_e^2 & 13L_e & -3L_e^2 \\ 54 & 13L_e & 156 & -22L_e \\ -13L_e & -3L_e^2 & -22L_e & 4L_e^2 \end{bmatrix}. \tag{5.17}$$

.

The mass and stiffness matrices obtained above are the mass and stiffness matrices for one element. In order to obtain the mass and stiffness matrices for the whole layer, mass and stiffness matrices of each element are assembled by adding the matrix components at the node which connects the two elements.

$$[K_{1+2}] = \frac{E_e I_e}{L_e^3} \begin{bmatrix} 12 & 6L_e & -12 & 6L_e & 0 & 0 \\ 6L_e & 4L_e^2 & -6L_e & 2L_e^2 & 0 & 0 \\ -12 & -6L_e & 12+12 & -6L_e+6L_e & -12 & 6L_e \\ 6L_e & 2L_e^2 & -6L_e+6L_e & 4L_e^2+4L_e^2 & -6L_e & 2L_e^2 \\ 0 & 0 & -12 & -6L_e & 12 & -6Le \\ 0 & 0 & 6L_e & 2L_e^2 & -6L_e & 4L_e^2 \end{bmatrix}. \tag{5.18}$$

$$[M_{1+2}] = \frac{\rho_e L_e}{420} \begin{bmatrix} 156 & 22L_e & 54 & -13L_e & 0 & 0 \\ 22L_e & 4L_e^2 & 13L_e & -3L_e^2 & 0 & 0 \\ 54 & 13L_e & 156+156 & -22L_e+22L_e & 54 & -13L_e \\ -13L_e & -3L_e^2 & -22L_e+22L_e & 4L_e^2+4L_e^2 & 13L_e & -3L_e^2 \\ 0 & 0 & 54 & 13L_e & 156 & -22L_e \\ 0 & 0 & -13L_e & -3L_e^2 & -22L_e & 4L_e^2 \end{bmatrix}. \tag{5.19}$$

A Matlab program is generated to construct global mass and stiffness matrices for the whole battery cell by assembling stiffness and mass matrices of all elements.

5.2 Dynamics Model of a Lithium-ion Battery Cell

The dynamics model of a LIB cell can be constructed by applying the equation of motion.

$$[M]\,\ddot{x}(t) + [C]\,\dot{x}(t) + [K]\,x(t) = f(t), \tag{5.20}$$

where f is the input force vector, [M]and [K]are the global mass and stiffness matrices of the battery cell, and$[C]$ is the damping matrix of the battery cell. The damping matrix of the whole battery cell can be obtained by using proportional damping equation which can express as:

$$[C] = \alpha\,[M] + \beta\,[K]\,, \tag{5.21}$$

where α & β are the damping coefficients.

In order to estimate the FRF of the model, Equation(5.20) is converted into the frequency domain using Laplace Transformation. Then, Equation(5.20) becomes:

$$[M]\,s^2X(s) + [C]\,sX(s) + [K]\,X(s) = F(s). \tag{5.22}$$

The transfer function of the system can be obtained as follow:

$$H(s) = \frac{X(s)}{F(s)} = \frac{1}{[M]\,s^2 + [C]\,s + [K]}. \tag{5.23}$$

The FRF of the system is the transfer function evaluated at $\mathrm{s} = \mathrm{j}\omega$. Thus, Equation(5.23) becomes:

$$H(j\omega) = \frac{1}{[M]\,(j\omega)^2 + [C]\,(j\omega) + [K]}. \tag{5.24}$$

$$H(j\omega) = \frac{1}{-\,[M]\,\omega^2 + [C]\,(j\omega) + [K]}. \tag{5.25}$$

The $H(j\omega)$ in Equation(5.25) represents the FRF of the system.

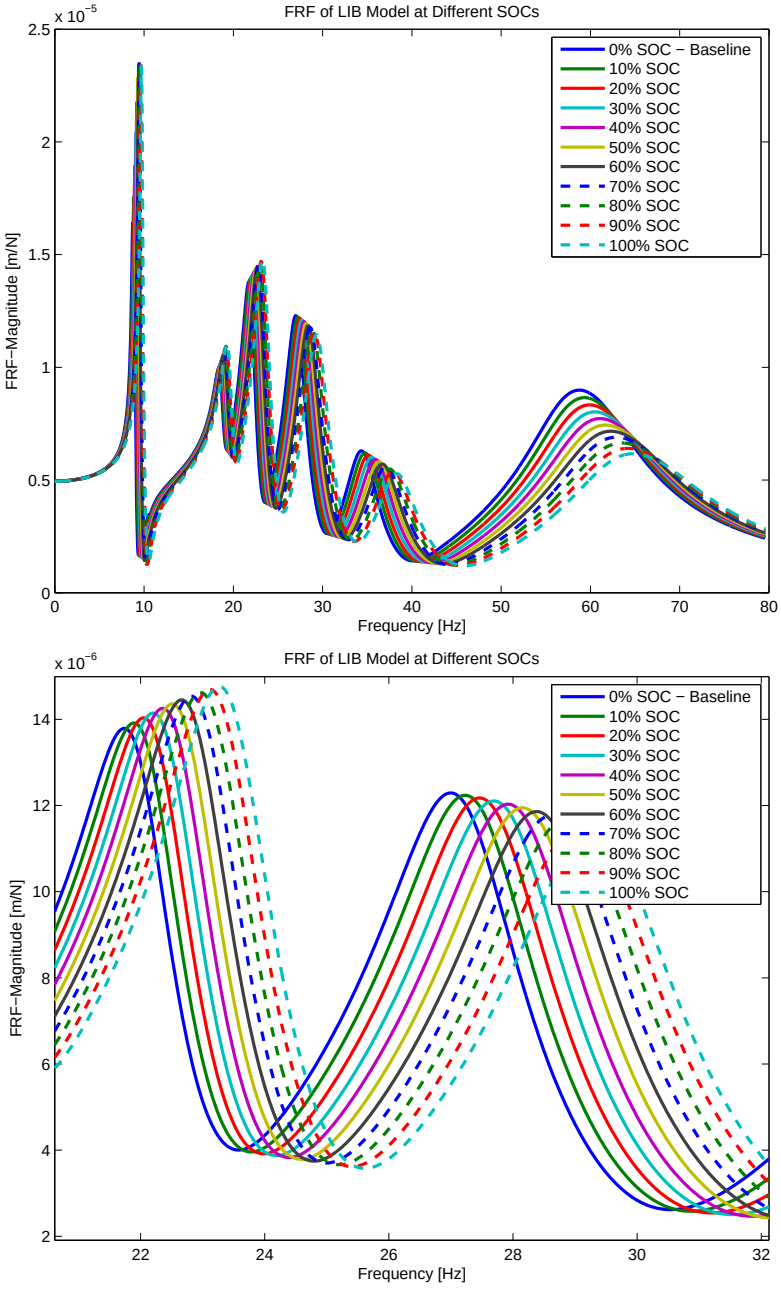

Figure 5.3: Dynamics Model of FRF with Constant Thickness Change.

5.3 Results

Figure 5.3 shows the FRFs from the analytical model of the LIB cell. The FRFs in this plot represent the simulation of the LIB during the charging cycle. The simulation

in this model is generated by changing the thickness of the electrodes. The model starts with the non-active electrodes' properties which is considered at 0% SOC. To bring the SOC in the model to 10% SOC, the original thickness of anode and cathode are ajusted with the estimated thickness change at 10% SOC. For charging cycle, the estimated value of Δh^- at 10% is added to the anode's thickness, and the estimated value of Δh^+ at 10% is subtracted from cathode thickness. Because of the losing ions in the cathode and the gaining ions in the anode during the charging cycle, thickness of the cathode decreases and thickness of the anode increases.

The results from the model show that the FRF shifts to a higher frequency as the SOC increases. The spaces between the FRFs are the same . This results confirm the hypothesis that electrodes' thickness will change during charge and discharge. When the battery cell is charged with constant current, there is constant change in thickness of every electrode. Also, when the battery cell is charged, anode's thickness increases while cathode's thickness decreases with constant values at different SOCs.

The FRFs plots from the vibration test and the analytical model are shown in Figure 5.4. The FRFs in both vibration test and model shift with the same spacing to the higher frequency as the SOC increases. However, the results from the test and model are not fully correlated. The FRFs from the model shows that the FRFs shift with the same spacing from 10% to 100%. The result from the test shows that the shifting in FRF at 90% and 100% is decreased. The spacing from 80% to 90% SOC is just around 40% of the previous one. The spacing from 90% to 100% is just half of the one from 80% to 90% SOC. It is assumed that the decrease in spacing between FRFs after 80% SOC is caused by the ions saturation in anode's material. When the anode material is saturated with Li-ions, it cannot absorb anymore ions from the cathode. Therefore, the increase in anode' thickness when the LIB cell reaches 90% and 100% SOCs will be less than the previous ones.

The model is used to verify the assumption of the ions saturation in the anode by reducing the thickness change of the anode at 90% and 100% SOCs. The thickness change of the electrodes are adjusted at 90% and 100% so that the increase in anode

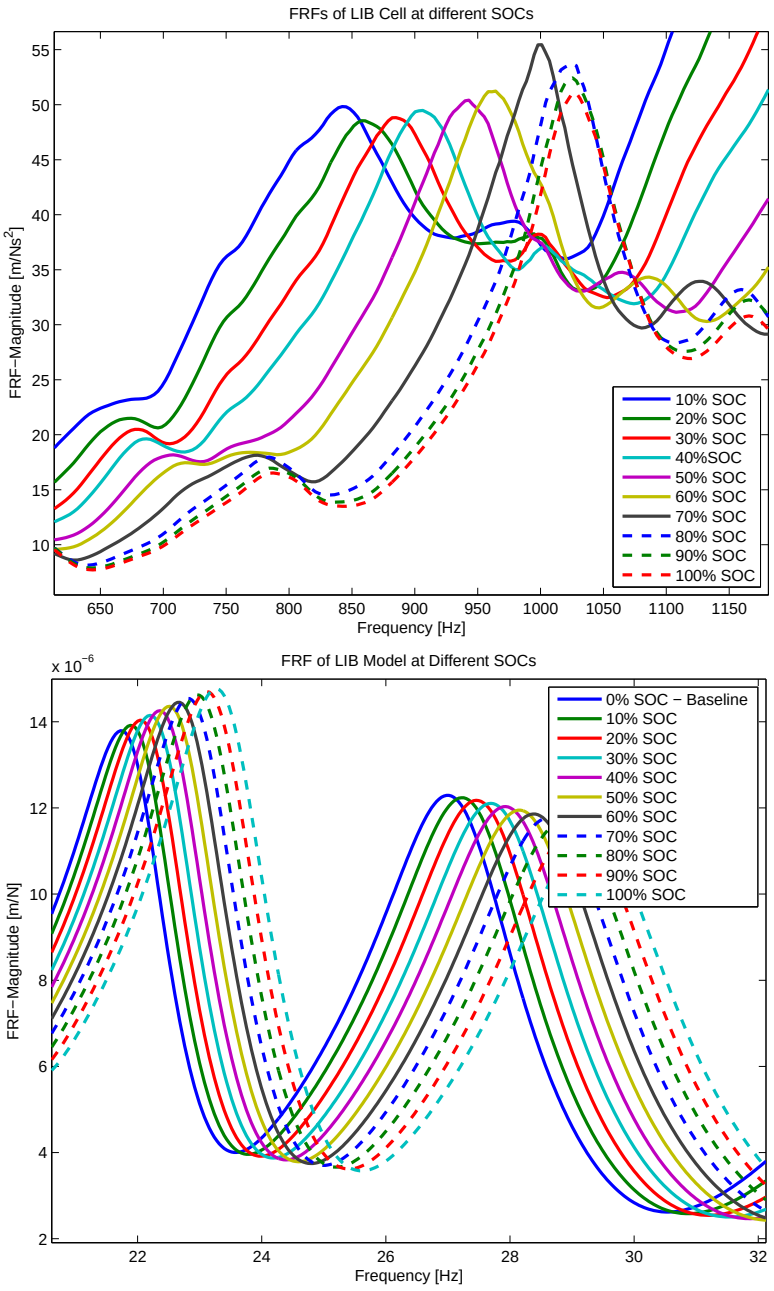

Figure 5.4: Compare FRFs Between Vibration Test and Model.

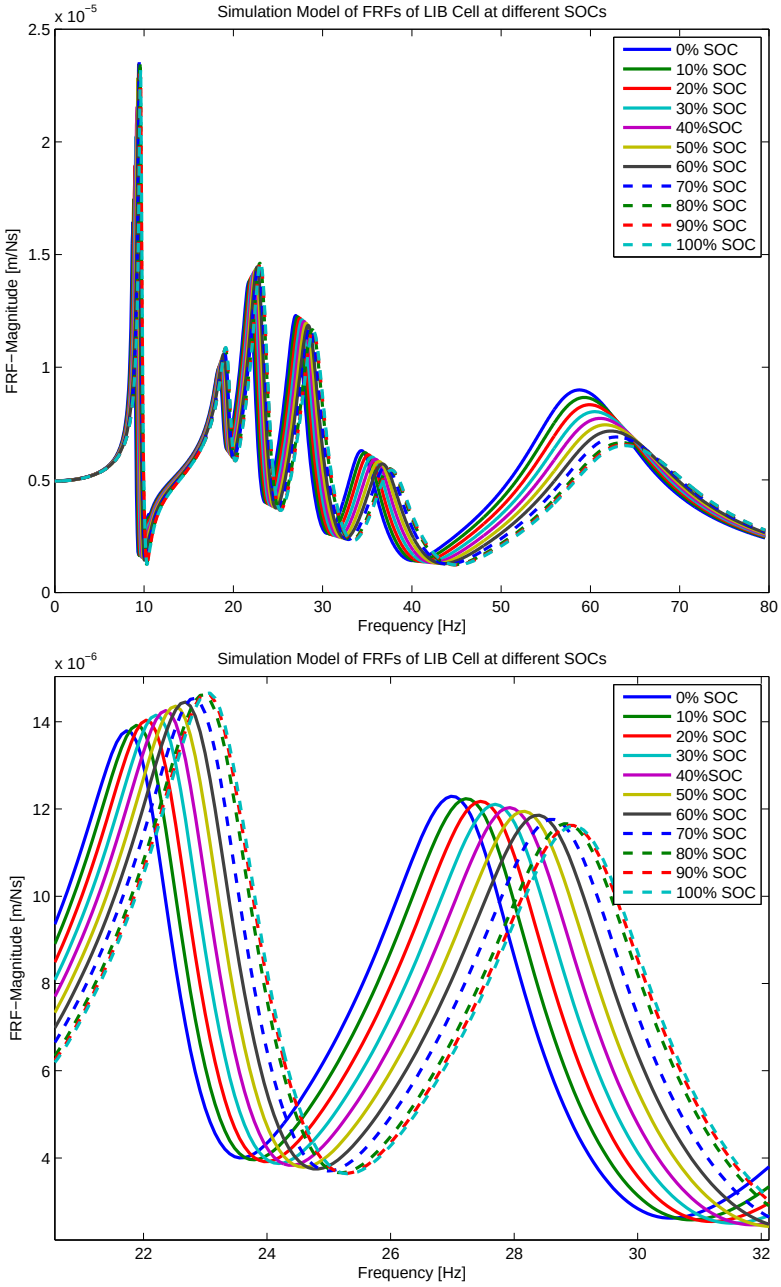

Figure 5.5: Dynamics Model with Adjusted Thickness Changes at 90% and 100% SOCs to Match the Vibration Test Results.

thickness from 80% to 90% is equal to 40% of Δh^-, and the increase in thickness from 90% to 100% is equal to 20% of Δh^-. The result of these adjustments is plotted in Figure 5.5.

The results from the adjusted FRF model show that the spacing between FRF at 90% and 100% decrease proportionally with the decreased thickness input. The results from the adjusted model are fully correlated with the results from the vibration test. The model has confirmed with the results from experiment that thickness of the electrodes increase with the same rate during charging process until the SOC reaches to 80%. After 80% SOC, electrodes' thickness will change with a smaller amount. This information indicates that the anode's material will be saturated with Li-ions when the LIB cell reaches 80% SOC. The same amount of Li-ions transport from cathode to anode after 80% SOC will result in an increase in anode's density, rather than in its volume. This information explains the fact that overcharging the battery cell will cause severe damage or destroy the cell when the increase in density will lead to the increase in stress. As a result, crack and rupture on the anode will occur.

6. CONCLUSIONS AND LIMITATIONS

6.1 Conclusions

Current technology cannot estimate the exact SOCs and SOHs of a LIB cell. The only way to obtain the exact SOCs of a LIB cell is measuring the constant current and time a LIB cell is charged or discharged. However, it is very difficult to track the current and time during service because the current always changes its value due to the types of applications and the working environment. SOCs estimation using other parameters such as voltage vs time, or voltage vs internal resistance are not reliable when they are dependent on the total capacity of the LIB cell. As the capacity of a LIB cell is degraded due to aging or damage, more error will occur. As a result, those estimation will be incorrect.

It is important to develop a method which can measure the exact SOCs of the battery cell. Such method can also be used to determine the SOHs of the cell because the SOC represents the capacity of the LIB cell. As a LIB cell loses its capacity, it cannot hold as much charge as it should be; thus, the capacity loss will reflect through the highest SOC of a LIB cell. In other words, the highest SOC of a bad LIB cell will be less than the highest SOC of a good one.

The goal of this thesis is to develop and demonstrate a method to diagnose the SOCs and SOHs of a LIB cell using vibration-based testing and modeling. The advantage of the vibration test is the ability to link the structural changes in a LIB cell to its SOCs. As the LIB cell changes its SOC, there are also changes in the cell's structure due to the changes in properties of the individual electrode inside the LIB cell. By capturing the FRFs of the battery cell's structure, the SOCs of the battery cell are obtained. Therefore, the SOHs of the LIB cell can be determined. The results from vibration test show that the test can describe the changes in electrodes' thickness

through changes in the LIB cell's FRFs. As the LIB cell increases in its SOC, the FRF of the battery cell is shifted to higher frequencies. Moreover, the amount of FRF shifting is directly related to the amount of thickness change in the anode. This information is very useful in determining when the anode is saturated with Li-ions. The saturation in the anode can be used to determine the maximum SOC of a LIB cell. When the spacing between FRFs starts to reduce in size, it indicates that the saturation occurs in the anode as the thickness of anode increase less than the ones from previous SOCs. The health of a LIB cell, which is under diagnosis, can be obtained by comparing the spacing of its FRFs to the one of the reference LIB cell. The reduce in spacing indicates the battery cell has lost it capacity. The difference in size of the FRFs spacing compare to the reference FRFs indicates that there is damage in the electrodes.

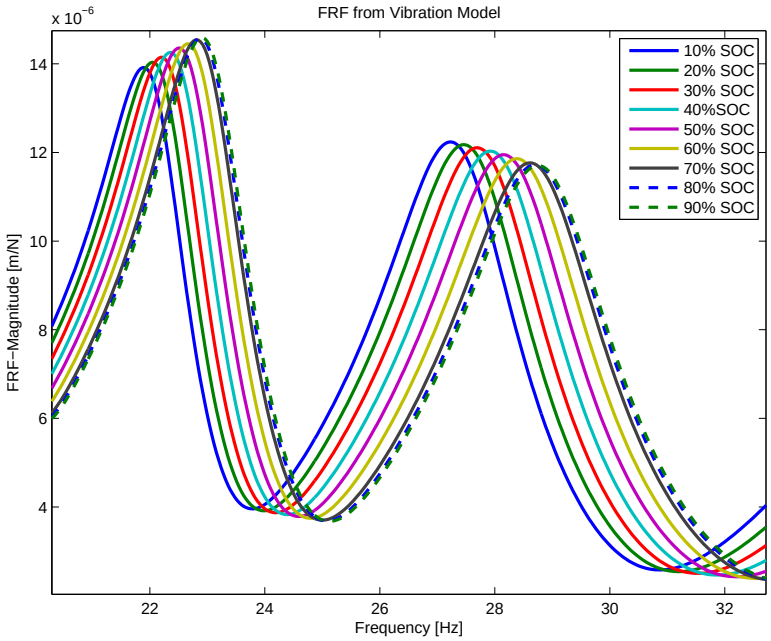

Figure 6.1: Simulation of LIB Cell Has It Anode Saturated at 70% SOC.

Figure 6.1 shows the simulation of a LIB cell which has its anode saturated at 70% SOC. The spacing in FRFs starts to decrease after the LIB cell reaches 70%

SOC. Therefore, this battery cell has lost around 10% of it total capacity since the healthy LIB cell's saturation is at 80% SOC.

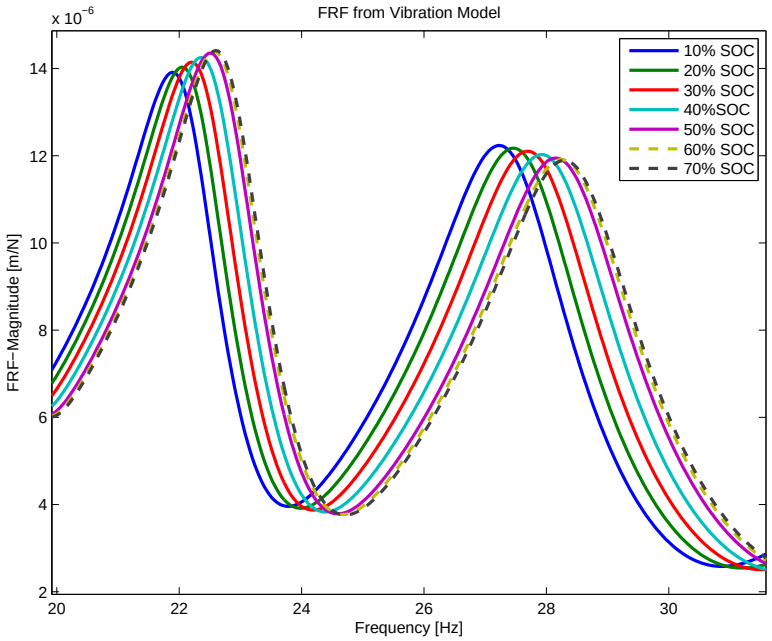

Figure 6.2: Simulation of LIB Cell Has the Anode Saturated at 50% SOC.

Figure 6.2 shows another simulation of a degraded LIB cell. In this case, the spacing in FRFs starts to decrease after the cell reaches 50% SOC. The result indicates this battery cell has lost 30% of its total capacity.

The analytical model of the LIB cell plays a critical role in determining the SOH of a LIB cell. First, results from the model are used to verify the results from the vibration test. The model proves that the shifting in FRFs is caused by the change in thickness of the anode. As the thickness of the anode is decreased in the model, the shifting in FRFs of the model is also decreased. Therefore, by changing the parameters in the model to obtain the similar results from the vibration test, the source of changes can be identified. Thus, this model can be used as a diagnosis tool to identify the problems of the LIB cell. Also, by introducing other degradation factors into the model, the model can also be used as a prognosis tool to predict the FRFs of the LIB cell in which those degradation factors present.

6.2 Limitations

There are limitations that need to be considered in order to improve the work in this study. First, FRFs of the LIB cell are obtained by applying the driving point measurement to the battery cell's structure. However, the driving point measurement is strictly dependent on the initial conditions of the location and the input excitation. As any one of those initial conditions is slightly changed, the results will be different. Therefore, in order to obtain similar results from different test objects, it is required the exact same excitation is applied on the exact same location on different test objects. Thus, it is difficult to eliminate the changes in the FRFs caused by the initial conditions.

Also, in order to investigate the effect of mechanical properties changes of the electrodes to the performance and health of the LIB cell, all other degradation factors such as temperature, age, damage, etc. are constrained. The testing environment is kept under ideal condition which all other factors are constants or eliminated. In practical applications, any of those factors can affect the test results which makes it difficult to distinguish the source of changes in FRFs. It is essential to introduce those degradation factors into the test setup to investigate the effect from each of them to the changes in FRFs of the LIB cell.

Finally, the analytical model has not included other factors that can cause degradation to the LIB cell other than the properties of the electrodes. By introducing each factor into the model, the differences in FRFs obtained can be used to identify and predict the actual problems of the battery which are obtained from the vibration tests.

LIST OF REFERENCES

LIST OF REFERENCES

[1] Masaki Yoshio, Ralph J Brodd, and Akiya Kozawa. *Lithium-ion batteries: science and technologies*. Springer, 2009.

[2] Thomas B Reddy. *Linden's Handbook of Batteries*, volume 4. McGraw-Hill, 2011.

[3] Martin Coleman, Chi Kwan Lee, Chunbo Zhu, and William Gerard Hurley. State-of-charge determination from emf voltage estimation: Using impedance, terminal voltage, and current for lead-acid and lithium-ion batteries. *Industrial Electronics, IEEE Transactions on*, 54(5):2550–2557, 2007.

[4] Sabine Piller, Marion Perrin, and Andreas Jossen. Methods for state-of-charge determination and their applications. *Journal of power sources*, 96(1):113–120, 2001.

[5] Ben Kenney, Ken Darcovich, Dean D MacNeil, and Isobel J Davidson. Modelling the impact of variations in electrode manufacturing on lithium-ion battery modules. *Journal of Power Sources*, 213:391–401, 2012.

[6] Claus Daniel. Materials and processing for lithium-ion batteries. *Jom*, 60(9):43–48, 2008.

[7] Nathan D Sharp. Lithium-ion battery electrode inspection using flash thermography. 2012.

[8] Madeleine Smith, R Edwin García, and Quinn C Horn. The effect of microstructure on the galvanostatic discharge of graphite anode electrodes in licoo2-based rocking-chair rechargeable batteries. *Journal of The Electrochemical Society*, 156(11):A896–A904, 2009.

[9] Xianming Wang, Yoshitsugu Sone, and Saburo Kuwajima. In situ investigation of the volume change in li-ion cell with charging and discharging satellite power applications. *Journal of The Electrochemical Society*, 151(2):A273–A280, 2004.

[10] Rujian Fu, Meng Xiao, and Song-Yul Choe. Modeling, validation and analysis of mechanical stress generation and dimension changes of a pouch type high power li-ion battery. *Journal of Power Sources*, 2012.

[11] Abdelhamid Guechaichia and Irina Trendafilova. A simple method for enhanced vibration-based structural health monitoring. In *Journal of Physics: Conference Series*, volume 305, page 012073. IOP Publishing, 2011.

[12] Douglas E Adams and Madhura Nataraju. A nonlinear dynamical systems framework for structural diagnosis and prognosis. *International Journal of Engineering Science*, 40(17):1919–1941, 2002.

[13] Vijay A Sethuraman, Nathan Van Winkle, Daniel P Abraham, Allan F Bower, and Pradeep R Guduru. Real-time stress measurements in lithium-ion battery negative-electrodes. *Journal of Power Sources*, 206:334–342, 2012.

[14] Dave Andre, Christian Appel, Thomas Soczka-Guth, and Dirk Uwe Sauer. Advanced mathematical methods of soc and soh estimation for lithium-ion batteries. *Journal of Power Sources*, 2012.

[15] Nader Jalili. *Piezoelectric-based vibration control: from macro to micro/nano scale systems*. Springer, 2010.

[16] Kandler Smith and Chao-Yang Wang. Power and thermal characterization of a lithium-ion battery pack for hybrid-electric vehicles. *Journal of power sources*, 160(1):662–673, 2006.

[17] Xinran Xiao, Wei Wu, and Xiaosong Huang. A multi-scale approach for the stress analysis of polymeric separators in a lithium-ion battery. *Journal of Power Sources*, 195(22):7649–7660, 2010.

[18] Mohammad Charkhgard and Mohammad Farrokhi. State-of-charge estimation for lithium-ion batteries using neural networks and ekf. *Industrial Electronics, IEEE Transactions on*, 57(12):4178–4187, 2010.

[19] MA Eltaher, Amal E Alshorbagy, and FF Mahmoud. Vibration analysis of euler-bernoulli nanobeams by using finite element method. *Applied Mathematical Modelling*, 2012.

[20] Jie Liu, Abhinav Saxena, Kai Goebel, Bhaskar Saha, and Wilson Wang. An adaptive recurrent neural network for remaining useful life prediction of lithium-ion batteries. Technical report, DTIC Document, 2010.

[21] Languang Lu, Xuebing Han, Jianqiu Li, Jianfeng Hua, and Minggao Ouyang. A review on the key issues for lithium-ion battery management in electric vehicles. *Journal of Power Sources*, 226:272–288, 2013.

[22] Valer Pop, Henk Jan Bergveld, PHL Notten, and Paul PL Regtien. State-of-the-art of battery state-of-charge determination. *Measurement Science and Technology*, 16(12):R93, 2005.

[23] Bhaskar Saha, Kai Goebel, Scott Poll, and Jon Christophersen. Prognostics methods for battery health monitoring using a bayesian framework. *Instrumentation and Measurement, IEEE Transactions on*, 58(2):291–296, 2009.

[24] J-M Tarascon and Michel Armand. Issues and challenges facing rechargeable lithium batteries. *Nature*, 414(6861):359–367, 2001.

[25] M Broussely, Ph Biensan, F Bonhomme, Ph Blanchard, S Herreyre, K Nechev, and RJ Staniewicz. Main aging mechanisms in li ion batteries. *Journal of Power Sources*, 146(1):90–96, 2005.

APPENDIX

APPENDIX: MATLAB CODES

```
% Huan Pham
% Finite element model for Non-Active cell (Zero charged)

clear all;
clc;
close all;

n=4;              % number of elements
m=4+(n-1)*2;      % matrix size of each layer
Kgap=3900;        % separator spring stiffness
Kair=0.001;           % bottom boundary stiffness/air compressibility
alpha=10e6;       % constant 1 for proportional damping
beta=10e-3;       % constant 2 for proportional damping
L=23.5e-3;        % length of electrode in m
t2=0.1e-3;        % thickness of single-sided cathode in m
E2=8.342e9;         % Young's modulus of single-sided cathode in Pa
t4=0.13e-3;       % thickness of double-sided anode in m
% t4=(0.13e-3)+(0.13e-3)*.1; %This is used for simulation when change the
% thickness of the anode
E4=3.442e9;          % Young's modulus of double-sided anode in Pa
t5=0.15e-3;       % thickness area of double-sided cathode in m
% t5=(0.15e-3)-(0.15e-3)*.1; %This is used for simulation when change the
% thickness of the cathode
E5=3.172e9;         % Young's modulus of double-sided cathode in Pa


%FEA for cover layer
E1=4.151e9; Ie1=(14.5e-3*0.0009^3)/12; rho1=585; Le1=L/n;
Ke1=E1*Ie1/Le1^3*[12 6*Le1 -12 6*Le1;6*Le1 4*Le1^2 -6*Le1 2*Le1^2;-12 -6*Le1 12 -6*
    Le1; 6*Le1 2*Le1^2 -6*Le1 4*Le1^2];
Me1=rho1*Le1/420*[156 22*Le1 54 -13*Le1;22*Le1 4*Le1^2 13*Le1 -3*Le1^2;54 13*Le1 156
    -22*Le1; -13*Le1 -3*Le1^2 -22*Le1 4*Le1^2];

Kg1=zeros(m,m);
Mg1=Kg1;

for i=0:n-1
Kg1(1+2*i:4+2*i,1+2*i:4+2*i)=Kg1(1+2*i:4+2*i,1+2*i:4+2*i)+Ke1;
```

```
Mg1(1+2*i:4+2*i,1+2*i:4+2*i)=Mg1(1+2*i:4+2*i,1+2*i:4+2*i)+Me1;
end;

%add Kgap to the diagonal in the stiffness matrix
for i=0:n
    Kg1(2*i+1,2*i+1)=Kg1(2*i+1,2*i+1)+Kgap;
end;

%-------------------------------------------------------------------------
%FEA for bottom cover
% for i=0:n-1
% Kg3(1+2*i:4+2*i,1+2*i:4+2*i)=Kg3(1+2*i:4+2*i,1+2*i:4+2*i)+Ke1;
% Mg3(1+2*i:4+2*i,1+2*i:4+2*i)=Mg3(1+2*i:4+2*i,1+2*i:4+2*i)+Me1;
% end;
Kg3=Kg1;
Mg3=Mg1;
%add boundary stiffness to the bottom layer as air stiffness
for i=0:n
    Kg3(2*i+1,2*i+1)=Kg3(2*i+1,2*i+1)+Kair;
end;

%-------------------------------------------------------------------------
%FEA for single-sided cathode
Ie2=(14.5e-3*t2^3)/12; rho2=2780; Le2=L/n;      % Density unit kg/m^3
Ke2=E2*Ie2/Le2^3*[12 6*Le2 -12 6*Le2;6*Le2 4*Le2^2 -6*Le2 2*Le2^2;-12 -6*Le2 12 -6*
    Le2; 6*Le2 2*Le2^2 -6*Le2 4*Le2^2];
Me2=rho2*Le2/420*[156 22*Le2 54 -13*Le2;22*Le2 4*Le2^2 13*Le2 -3*Le2^2;54 13*Le2 156
    -22*Le2; -13*Le2 -3*Le2^2 -22*Le2 4*Le2^2];

Kg2=zeros(m,m);
Mg2=Kg2;

for i=0:n-1
Kg2(1+2*i:4+2*i,1+2*i:4+2*i)=Kg2(1+2*i:4+2*i,1+2*i:4+2*i)+Ke2;
Mg2(1+2*i:4+2*i,1+2*i:4+2*i)=Mg2(1+2*i:4+2*i,1+2*i:4+2*i)+Me2;
end;

%add 2Kgap to diagonal in the stiffness matrix of cathode
for i=0:n
    Kg2(2*i+1,2*i+1)=Kg2(2*i+1,2*i+1)+2*Kgap;
end;

%-------------------------------------------------------------------------
%FEA for double-sided anode
```

```
Ie4=(14.5e-3*t4^3)/12; rho4=1885; Le4=L/n;
Ke4=E4*Ie4/Le4^3*[12 6*Le4 -12 6*Le4;6*Le4 4*Le4^2 -6*Le4 2*Le4^2;-12 -6*Le4 12 -6*
    Le4; 6*Le4 2*Le4^2 -6*Le4 4*Le4^2];
Me4=rho4*Le4/420*[156 22*Le4 54 -13*Le4;22*Le4 4*Le4^2 13*Le4 -3*Le4^2;54 13*Le4 156
    -22*Le4; -13*Le4 -3*Le4^2 -22*Le4 4*Le4^2];

Kg4=zeros(4+(n-1)*2,4+(n-1)*2);
Mg4=Kg4;

for i=0:n-1
Kg4(1+2*i:4+2*i,1+2*i:4+2*i)=Kg4(1+2*i:4+2*i,1+2*i:4+2*i)+Ke4;
Mg4(1+2*i:4+2*i,1+2*i:4+2*i)=Mg4(1+2*i:4+2*i,1+2*i:4+2*i)+Me4;
end;

%add 2Kgap to each node in the stiffness matrix of anode
for i=0:n
    Kg4(2*i+1,2*i+1)=Kg4(2*i+1,2*i+1)+2*Kgap;
end;

%-------------------------------------------------------------------------
%FEA for double-sided cathode
Ie5=(14.5e-3*t5^3)/12; rho5=2813; Le5=L/n;
Ke5=E5*Ie5/Le5^3*[12 6*Le5 -12 6*Le5;6*Le5 4*Le5^2 -6*Le5 2*Le5^2;-12 -6*Le5 12 -6*
    Le5; 6*Le5 2*Le5^2 -6*Le5 4*Le5^2];
Me5=rho5*Le5/420*[156 22*Le5 54 -13*Le5;22*Le5 4*Le5^2 13*Le5 -3*Le5^2;54 13*Le5 156
    -22*Le5; -13*Le5 -3*Le5^2 -22*Le5 4*Le5^2];

Kg5=zeros(4+(n-1)*2,4+(n-1)*2);
Mg5=Kg5;

for i=0:n-1
Kg5(1+2*i:4+2*i,1+2*i:4+2*i)=Kg5(1+2*i:4+2*i,1+2*i:4+2*i)+Ke5;
Mg5(1+2*i:4+2*i,1+2*i:4+2*i)=Mg5(1+2*i:4+2*i,1+2*i:4+2*i)+Me5;
end;

%add 2Kgap to each node in the stiffness matrix of double-side cathode
for i=0:n
    Kg5(2*i+1,2*i+1)=Kg5(2*i+1,2*i+1)+2*Kgap;
end;


%-------------------------------------------------------------------------
%Construct stiffness matrix for sequence layers with 11 anodes and 11 cathodes
%total of 22 layers (11 cathodes, 11 anodes)
```

```
K1=zeros(m*2,m*2);
K1(1:m,1:m)=K1(1:m,1:m)+Kg4;
K1(m+1:2*m,m+1:2*m)=K1(m+1:2*m,m+1:2*m)+Kg5;

K2=zeros(m*22,m*22);
for i=0:10
    K2((2*m*i+1:2*m*(i+1)),(2*m*i+1:2*m*(i+1)))=K2((2*m*i+1:2*m*(i+1)),(2*m*i+1:2*m*(
        i+1)))+K1;
end;

%Construct stiffness matrix for whole battery (27 layers)
global K3;
K3=zeros(m*27,m*27);
K3(1:m,1:m)=K3(1:m,1:m)+Kg1;     %top cover layer
K3(m+1:2*m,m+1:2*m)=K3(m+1:2*m,m+1:2*m)+Kg2;     %single_sided cathode
K3(2*m+1:24*m,2*m+1:24*m)=K3(2*m+1:24*m,2*m+1:24*m)+K2; %22 layers of double_sided
    anodes and double_sided cathodes
K3(24*m+1:m*25,24*m+1:m*25)=K3(24*m+1:m*25,24*m+1:m*25)+Kg4;     %double_sided anode
K3(25*m+1:26*m,25*m+1:26*m)=K3(25*m+1:26*m,25*m+1:26*m)+Kg2;     %single_sided cathode
K3(26*m+1:27*m,26*m+1:27*m)=K3(26*m+1:27*m,26*m+1:27*m)+Kg3;     %bottom cover layer

%add -Kgap to the connected nodes in the matrix
for i=0:(m/2)*26-1
    K3(m+(2*i+1),(2*i+1))=K3(m+(2*i+1),1+(2*i+1))-Kgap;
    K3((2*i+1),m+(2*i+1))=K3(1+(2*i+1),m+(2*i+1))-Kgap;
end


%-------------------------------------------------------------------------
%-------------------------------------------------------------------------
% Construct mass matrix for sequence layers with 11 anodes and 11 cathodes
% total of 44 layers (11 cathodes, 11 anodes, 22 separators)
M1=zeros(m*2,m*2);
M1(1:m,1:m)=M1(1:m,1:m)+Mg4;
M1(m+1:2*m,m+1:2*m)=M1(m+1:2*m,m+1:2*m)+Mg5;

M2=zeros(m*22,m*22);
for i=0:10
    M2((2*m*i+1:2*m*(i+1)),(2*m*i+1:2*m*(i+1)))=M2((2*m*i+1:2*m*(i+1)),(2*m*i+1:2*m*(
        i+1)))+M1;
end;

%Construct mass matrix for whole battery (27 layers)
```

```
global M3;
M3=zeros(m*27,m*27);
M3(1:m,1:m)=M3(1:m,1:m)+Mg1;     %top cover layer
M3(m+1:2*m,m+1:2*m)=M3(m+1:2*m,m+1:2*m)+Mg2;     %single_sided cathode
M3(2*m+1:24*m,2*m+1:24*m)=M3(2*m+1:24*m,2*m+1:24*m)+M2; %22 layers of double_sided
    anodes and double_sided cathodes
M3(24*m+1:m*25,24*m+1:m*25)=M3(24*m+1:m*25,24*m+1:m*25)+Mg4;     %double_sided anode
M3(25*m+1:26*m,25*m+1:26*m)=M3(25*m+1:26*m,25*m+1:26*m)+Mg2;     %single_sided cathode
M3(26*m+1:27*m,26*m+1:27*m)=M3(26*m+1:27*m,26*m+1:27*m)+Mg1;     %bottom cover layer

%_____________________________________________________________________

%Damping Matrix
C=0.000005*M3+0.00005*K3;

w=0:0.15:500;
for ii=1:max(size(w))
    HH(:,:,ii)=inv(-w(ii)^2*M3+1j*w(ii)*C+K3);
end
%Plot the FRF
figure;
plot(w/2/pi,abs(squeeze(HH(1,1,:))),'k-');
xlabel('Frequency [Hz]');
ylabel('|H_{11}| [m/N]');
```

VITA

VITA

Huan Le Pham was born in Viet Nam. In 2003, he moved to Oklahoma City, Oklahoma in the United States with his family. He earned his Bachelor of Science in Mechanical and Aerospace Engineering from Oklahoma State University in Stillwater, Oklahoma, graduating with Magna Cum Laude in May 2011. He has joined Sandia National Laboratories (SNL) in August 2011 and participated in the Critical Skill Master Program (CSMP) which provides him the financial aid to obtain the master degree in science and engineering. In January 2012, he came to Purdue in West Lafayette, Indiana, to pursue the Master of Science in Mechanical Engineering (MSME)under the guidance of Dr. Douglas E. Adams. The focus of his work is utilizing the vibration-based testing method to monitor the health of a Lithium-ion battery cell. He is expecting to graduate in December 2013 with the MSME. After completing the program, he will return to SNL to continue his work to contribute in strengthening the national security of the United States.